© 2015. Published by The Company of Biologists Ltd | Development (2015) 142, 2740-2751 doi:10.1242/dev.119339

RESEARCH ARTICLE

STEM CELLS AND REGENERATION

Scalloped and Yorkie are required for cell cycle re-entry of quiescent cells after tissue damage

Joy H. Meserve[1] and Robert J. Duronio[1,2,3,4,*]

ABSTRACT

Regeneration of damaged tissues typically requires a population of active stem cells. How damaged tissue is regenerated in quiescent tissues lacking a stem cell population is less well understood. We used a genetic screen in the developing *Drosophila melanogaster* eye to investigate the mechanisms that trigger quiescent cells to re-enter the cell cycle and proliferate in response to tissue damage. We discovered that Hippo signaling regulates compensatory proliferation after extensive cell death in the developing eye. Scalloped and Yorkie, transcriptional effectors of the Hippo pathway, drive Cyclin E expression to induce cell cycle re-entry in cells that normally remain quiescent in the absence of damage. Ajuba, an upstream regulator of Hippo signaling that functions as a sensor of epithelial integrity, is also required for cell cycle re-entry. Thus, in addition to its well-established role in modulating proliferation during periods of tissue growth, Hippo signaling maintains homeostasis by regulating quiescent cell populations affected by tissue damage.

KEY WORDS: *Drosophila*, Cell cycle, Quiescence, Apoptosis, Compensatory proliferation, Regeneration, Hippo signaling

INTRODUCTION

Tissue regeneration has fascinated biologists for many years, but the molecular mechanisms underlying this process have only recently begun to be understood. Pioneering experiments on regenerating hydra by the Abbé Trembley in the 1700s and on other organisms in the 1800s (Morgan, 1901) established that regeneration functions as a reparative process to replace tissues damaged by injury or disease and occurs as a restorative process to repair old and damaged tissues throughout an organism's life. Although early experiments on highly regenerative animals, such as hydra, are fundamental for our understanding of regeneration, the lack of facile genetic manipulation in these organisms made identifying molecular mechanisms difficult.

In the 1970s, *Drosophila melanogaster* emerged as a powerful and genetically tractable experimental system in which to study regeneration. Larval imaginal discs, which are epithelial tissues that proliferate during larval life and differentiate during pupation into adult structures, are able to regrow after substantial tissue loss due to irradiation or removal of fragments by surgery (Bryant, 1971; Haynie and Bryant, 1977; Worley et al., 2012). In these imaginal discs, a process called compensatory proliferation (CP) replaces cells lost by tissue damage. Research from several laboratories in the last decade has elucidated some of the mechanisms controlling CP. One important mechanism is the induction of proliferation by apoptotic cells. Caspases are required for robust regeneration in many organisms even though caspase activity and cell death contributes to initial tissue loss following damage. When apoptosis is blocked by the baculovirus effector-caspase inhibitor p35 in damaged *Drosophila* wing discs, 'undead cells', which have initiated but not completed apoptosis, induce hyperproliferation (Huh et al., 2004; Perez-Garijo et al., 2004). This hyperproliferation is dependent on the initiator caspase Dronc, suggesting that this caspase has a role in inducing proliferation independently of apoptosis (Huh et al., 2004). Proliferation induced by undead cells or genuine apoptotic cells may act in various contexts through multiple pathways, including the Wingless/Wnt, Dpp/BMP, Jun N-terminal kinase (JNK), and Hedgehog signaling pathways (Ryoo et al., 2004; Perez-Garijo et al., 2005; Fan and Bergmann, 2008). Apoptosis-induced proliferation involving mitogenic signaling is likely to be just one part of a larger pathway controlling CP (Mollereau et al., 2013).

The participation of apoptotic cells in regeneration is not unique to *Drosophila*. Studies in other organisms have revealed that caspase activity is required for regeneration in the *Xenopus laevis* tadpole tail (Tseng et al., 2007) and in the mammalian liver and skin (Li et al., 2010). Additionally, many of the pathways identified as being involved in CP regulation in *Drosophila* are also involved in vertebrate tissue repair. For example, both the Hedgehog (Cai et al., 2011) and JNK (Wuestefeld et al., 2013) pathways are required for mammalian liver regeneration, and Wnt signaling is required for limb regeneration in *Xenopus*, axolotl and zebrafish (Kawakami et al., 2006). Thus, there are conserved mechanisms for regeneration between invertebrates and vertebrates.

How the cell cycle is regulated during regeneration to ensure proper regrowth remains unclear. Tissue regrowth can be accomplished by increasing proliferation to restore cell number, as in *Drosophila* wing discs, or by cellular growth without cell division, such as during endoreplication (Fox and Duronio, 2013). A strong proliferative response to damage occurs during planaria body regeneration (Wenemoser and Reddien, 2010), zebrafish heart regeneration (Poss et al., 2002) and *Xenopus* tail regeneration (Tseng et al., 2007), and endoreplication contributes to tissue repair in the mammalian liver (Sigal et al., 1999) and the *Drosophila* ovary (Tamori and Deng, 2013). In these tissues, a moderate increase in proliferating or endoreplicating cells quickly replaces lost tissue.

By contrast, how cell cycle exit in quiescent tissues is overcome to allow proliferation following damage is unclear. Robust inhibition of cell cycle re-entry in quiescent tissues is necessary to maintain tissue homeostasis and prevent neoplasia and cancer. Cell cycle inhibition thus presents a high hurdle to overcome before regeneration can take place. We investigated this issue using the *Drosophila* eye imaginal disc. The eye disc contains a

[1]Curriculum in Genetics & Molecular Biology, University of North Carolina, Chapel Hill, NC 27599, USA. [2]Integrative Program for Biological and Genome Sciences, University of North Carolina, Chapel Hill, NC 27599, USA. [3]Departments of Biology and Genetics, University of North Carolina, Chapel Hill, NC 27599, USA. [4]Lineberger Comprehensive Cancer Center, University of North Carolina, Chapel Hill, NC 27599, USA.

*Author for correspondence (duronio@med.unc.edu)

Received 4 November 2014; Accepted 29 June 2015

Development (2015) 142, 2740-2751 doi:10.1242/dev.119339

population of cells that are normally quiescent but will undergo cell cycle re-entry after induction of massive cell death (Fan and Bergmann, 2008). We used the developing eye as a model for CP and performed a genetic screen to identify regulators of this process. With this approach, we identified the transcription factor Scalloped (Sd) as a novel CP regulator. We show that Sd and the Sd binding partner Yorkie (Yki) are required for cell cycle re-entry following damage in the eye imaginal disc. Yki is a transcriptional effector of the Hippo pathway and was previously identified as a CP regulator in wing discs (Sun and Irvine, 2011; Grusche et al., 2011). We also found that CP in the eye disc requires the Hippo pathway regulator Ajuba (Jub), similar to recent results in the wing disc (Sun and Irvine, 2013). However, Jub activation during CP is likely to be differentially regulated in these two tissues. Our study demonstrates that Hippo signaling is required for quiescent cells to re-enter the cell cycle following tissue damage and is likely to provide insight into a variety of regenerative systems, particularly those within non-proliferative tissues.

RESULTS

Quiescent cells re-enter the cell cycle after tissue damage in the developing eye

The developing *Drosophila* eye is ideal for studying regeneration in a quiescent cell population. Many genetic tools are available for manipulating the eye imaginal disc, and subtle defects in eye development are readily apparent in the highly organized adult eye (Dominguez and Casares, 2005; Gutierrez-Avino et al., 2009). The neurocrystalline lattice of the *Drosophila* eye takes shape by precise control of the cell cycle and differentiation during development (Fig. 1A,L). In early larval development, the eye disc grows as undifferentiated cells proliferate asynchronously. During the third and last larval stage, a wave of differentiation associated with an apical constriction of the epithelial sheet called the morphogenetic furrow (MF) moves from posterior to anterior across the disc. Cells within the MF arrest in G1, and a subset begin to differentiate into photoreceptors. After the MF has passed, the remaining undifferentiated cells synchronously enter S phase in what is termed the second mitotic wave (SMW) (Fig. 1B). After the SMW, these cells become quiescent and await cues to differentiate (Fig. 1L) (Firth and Baker, 2005). This population is considered to be quiescent as very few cells posterior to the SMW enter S phase (Fig. 1B′) or undergo mitosis (Baker and Yu, 2001). Cells remain quiescent by mechanisms that prevent cell cycle re-entry, including CDK inhibition by Dacapo and E2f1 repression by Retinoblastoma-family protein (Rbf) (Buttitta et al., 2007; Ruggiero et al., 2012), as well as destruction of cell cycle regulators by the anaphase-promoting complex (Buttitta et al., 2010; Bandura et al., 2013).

Although cells posterior to the SMW are normally quiescent, cell cycle re-entry occurs after tissue damage (Fan and Bergmann, 2008). Expression of the pro-apoptotic gene *hid* with the *GMR* promoter, which is expressed posterior to the MF (supplementary material Fig. S1A), induces extensive cell death (Fig. 1E,F). Dying,

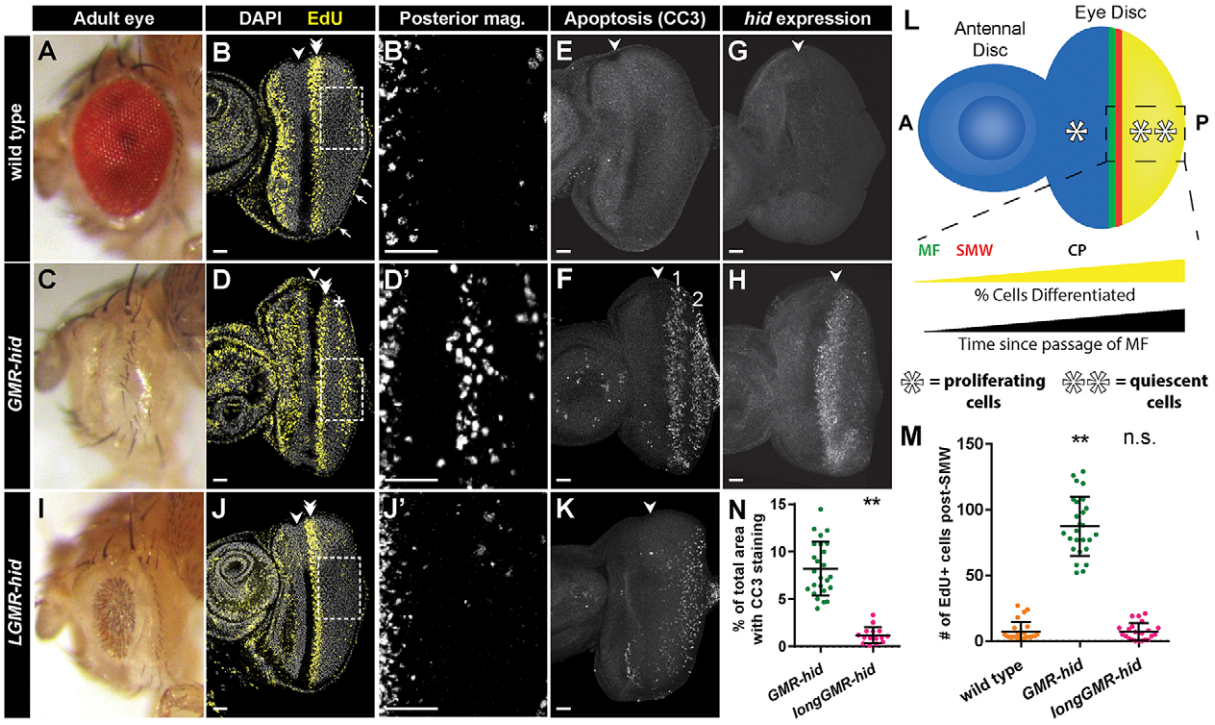

Fig. 1. Hid expression induces CP in the eye imaginal disc. (A,C,I) Adult eyes of the indicated genotypes. Wild-type (A) is *Oregon R*. (B,D,J) DAPI (DNA; single confocal slice in gray) and EdU (S phase; projection in yellow) staining of eye imaginal discs, indicating the MF (arrowheads) and the SMW (double arrowheads), respectively. Note that EdU^{+} cells in the row of cells around the disc (arrows in B) are margin cells and not part of the disc proper. Asterisk denotes CP (D). Boxes indicate areas of magnification shown in B′D′,J′. (E,F,K) Cleaved Caspase-3 (CC3) staining of apoptotic cells in discs of the indicated genotypes. The first (1) and second (2) apoptotic waves are indicated in (F). (G,H) *In situ* hybridization for *hid* mRNA in the indicated genotypes. (L) The eye disc, attached to the anterior (A) antennal disc, is composed of undifferentiated, proliferating cells (blue) anterior to the MF (green) and both undifferentiated and differentiated quiescent cells (yellow) posterior (P) to the SMW (red). Cells furthest from the MF (most posterior) are the most differentiated. (M) Quantification of CP in the indicated genotypes. All post-SMW, EdU^{+} eye disc cells were counted. Each circle represents the number of cells counted for a single disc, and bars represent mean and one standard deviation. For each genotype, $n \geq 22$ discs. $^{**}P=2.6\times10^{-17}$. (N) Quantification of percentage of total disc area with CC3 staining. Each circle represents the percentage for a single disc, and bars represent mean and one standard deviation. $n>15$ discs. $^{**}P=2.4\times10^{-14}$. n.s., not significant. Anterior is oriented to the left. Scale bars: 20 µm.

Development (2015) 142, 2740-2751 doi:10.1242/dev.119339

caspase-positive cells with pyknotic nuclei are extruded from the basal surface of the eye disc (supplementary material Fig. S1B,C), as in other discs (Gibson and Perrimon, 2005; Shen and Dahmann, 2005). Not all cells posterior to the SMW die, and some overcome cell cycle inhibition and re-enter S phase in a wave of proliferation (Fig. 1D,D′; Fan and Bergmann, 2008). *GMR-hid* flies are nearly eyeless (Fig. 1C), indicating that increased proliferation cannot fully compensate for tissue loss, probably because *GMR-hid* expression during pupal stages induces extensive apoptosis after the potential to re-enter the cell cycle is lost. Thus, *GMR-hid* eye discs behave somewhat differently compared with previous CP models in the wing where tissue regrowth is more complete (Mollereau et al., 2013). Nonetheless, tissue damage-induced cell cycle re-entry in the eye disc provides a valuable model for studying CP in a quiescent cell population.

Because apoptotic cells play a crucial role during CP, we further characterized the relationship between dying and proliferating cells in the eye disc. Rather than uniform apoptosis across *GMR-hid* discs, two distinct waves of cleaved Caspase-3 (CC3)-positive cells occur on either side of the CP wave (Fig. 1E,F; supplementary material Fig. S1D-E). Because CP overlaps substantially with the apoptosis-free zone between the two waves of CC3 staining, it was previously suggested that proliferating cells might inhibit apoptosis (Fan and Bergmann, 2008). However, these two waves of apoptosis persist when CP is blocked (see below and Fig. 3B,C), suggesting that CP does not inhibit apoptosis. Rather, variations in Hid activity across the disc may account for the observed pattern of apoptosis. Hid accumulation and activity varies posterior to the MF (Fan and Bergmann, 2014). In addition, *hid* mRNA is not uniformly expressed across *GMR-hid* discs, with high levels immediately posterior to the MF and lower levels more posteriorly (Fig. 1G,H). *hid* mRNA can be regulated by the miRNA *bantam* (*ban*) (Brennecke et al., 2003), which protects cells from apoptosis in certain damaged tissues after being upregulated by a Tie-like receptor tyrosine kinase (Tie)-dependent mechanism (Bilak et al., 2014). We did not detect *ban* induction in *GMR-hid* discs (supplementary material Fig. S5C), and *Tie* RNAi does not affect the pattern of apoptosis (supplementary material Fig. S2A). These results suggest that Tie-dependent *ban* induction is not responsible for decreased *hid* transcripts in the posterior eye disc.

Because *hid* transcripts are low in the posterior of the disc, we considered the possibility that dying cells in the first apoptotic wave promote apoptosis-induced apoptosis (AiA), resulting in the second apoptotic wave. AiA is mediated by JNK signaling (Perez-Garijo et al., 2013). However, expression of a dominant-negative version of the *Drosophila* JNK homolog Basket (Bsk) does not affect the pattern of apoptosis in *GMR-hid* discs (supplementary material Fig. S2B). Interestingly, although JNK signaling is required for CP in the wing disc (Ryoo et al., 2004), expression of Bsk^{DN} or Puckered (Puc), a negative regulator and downstream target of the JNK pathway, does not suppress CP (supplementary material Fig. S2C,D,G). Additionally, although *puc* is induced after damage in the wing (Bergantinos et al., 2010), *puc-lacZ* is not induced in *GMR-hid* eye discs (supplementary material Fig. S2E,F). We conclude from these data that regulation of Hid expression and activity, rather than S-phase entry, *ban* induction, or AiA, determines the pattern of apoptosis in *GMR-hid* discs and that JNK signaling is not a major CP regulator posterior to the MF.

Next, we explored contributions to the pattern of CP in *GMR-hid* discs. CP occurs in a well-defined wave that does not typically extend to the posterior edge of the disc (Fig. 1D,D′). Undifferentiated cells, which are the only cells that re-enter S phase in *GMR-hid* discs (Fan and Bergmann, 2008), are present at the posterior edge of the eye disc. We hypothesized that cells lose the competency to re-enter S phase prior to differentiation, perhaps owing to prolonged quiescence. To address this hypothesis, we shifted the wave of apoptosis towards the posterior edge of the disc by expressing *hid* under the control of *longGMR* (*LGMR*), a version of the *GMR* promoter that contains a repressor element and is only expressed in a subset of photoreceptors (Wernet et al., 2003; supplementary material Fig. S1F). Although we were unable to obtain clear *hid* mRNA signal in this genotype, probably owing to lower levels of accumulation than in *GMR-hid* discs, we did observe a single wave of apoptosis in the posterior region of *LGMR-hid* discs (Fig. 1K). In addition, *LGMR* flies have a reduced adult eye phenotype similar to, but less severe than, *GMR-hid* flies (Fig. 1I). Unlike in *GMR-hid* discs, however, CP is not induced in *LGMR-hid* discs (Fig. 1J,J′,M). This result is consistent with the idea that undifferentiated cells at the posterior of the disc are refractory to cell cycle re-entry in response to tissue damage. Alternatively, lower levels of apoptosis in *LGMR-hid* discs compared with *GMR-hid* discs (Fig. 1N) may not be sufficient to induce CP.

An RNAi screen identifies genes required for compensatory proliferation

How do undifferentiated cells overcome quiescence to re-enter the cell cycle in response to tissue damage? The mechanisms that control CP in quiescent eye discs are distinct from those in proliferating wing discs (Fan and Bergmann, 2008). For example, JNK signaling is required for CP in the wing disc (Ryoo et al., 2004) whereas our data suggest it is not required in the eye disc (supplementary material Fig. S2). To identify pathways necessary for cell cycle re-entry in the regenerating eye, we designed a genetic screen based on adult eye phenotypes. We expressed hairpin RNAs targeting individual genes in *GMR-hid* eye discs using the GAL4/UAS system and assessed the effect on CP by scoring the adult eye phenotype. To drive UAS-transgene expression, we constructed a *GMR-hid, GMR-Gal4/+* (*GMR>hid, Gal4*) line (unless otherwise noted, genotypes written as *GMR>hid, transgene* are heterozygous for *GMR-hid, GMR-Gal4*, and a UAS-transgene). Eyes in *GMR>hid, Gal4* flies are drastically reduced in size compared with wild type but larger than *GMR-hid* eyes (compare Fig. 1A,C and Fig. 2A). *GMR>hid, Gal4* larval eye discs exhibit strong CP (Fig. 2A′) with similar numbers of cells re-entering S phase compared with *GMR-hid* (P=0.39). We tested whether inhibiting CP would result in a detectable adult eye phenotype by expressing the mammalian CDK inhibitor p21 or dsRNA targeting *Cyclin E* in *GMR>hid, Gal4* eye discs. In these genotypes, CP is blocked and a reproducible adult eye phenotype results in which pigment is reduced (Fig. 2B-C′). Because pigment cells are one of the last cell types to differentiate, this result suggests that the undifferentiated, precursor pool is reduced when CP is blocked and that cells that undergo CP contribute to the adult eye. Importantly, the SMW does not appear to be affected in *GMR-Gal4, GMR-hid/UAS-p21* discs (supplementary material Fig. S3A,B), in contrast to *GMR-p21* flies in which the SMW is ablated (supplementary material Fig. S3C; de Nooij and Hariharan, 1995). These data suggest that the accumulation of Gal4 required to drive high UAS-transgene expression does not occur until posterior to the SMW, allowing us to assess phenotypes during CP without confounding defects in the SMW. In addition, these data indicate that we can detect loss of CP by monitoring adult eye phenotypes.

Development (2015) 142, 2740-2751 doi:10.1242/dev.119339

Using this approach, we screened a collection of UAS-RNAi lines targeting *Drosophila* transcription factors. Our rationale for this strategy is that many signaling pathways affecting cell cycle entry and CP have transcriptional output. In addition, multiple inputs can result in activation of the same transcription factor, and we reasoned that knocking down the transcription factor itself would result in a stronger phenotype than knocking down an upstream component. Of the 544 transcription factors included in both the Fly Transcription Factor Database (Pfreundt et al., 2010) and the Animal Transcription Factor Database (Zhang et al., 2012), we tested the 373 genes for which there was an available RNAi line (supplementary material Table S1). In our primary screen, candidate genes were identified based on suppression or enhancement of the *GMR>hid, Gal4* adult eye phenotype (Fig. 2D). *luciferase* (*luc*) RNAi was used as a negative control. Twelve UAS-RNAi lines caused lethality with both *GMR>hid, Gal4* and *GMR-Gal4* alone and were not examined further (supplementary material Table S1).

Fifty two UAS-RNAi lines modified the *GMR>hid, Gal4* adult eye phenotype: three acted as suppressors, including *glass*, which binds to and activates *GMR* (Fig. 2E; supplementary material Fig. S4); twelve displayed a small eye (Enhancer Category I; Fig. 2F; supplementary material Fig. S4); seven displayed moderate pigment loss (Enhancer Category II; Fig. 2G; supplementary material Fig. S4); twenty one displayed mild pigment loss (Enhancer Category III; Fig. 2H; supplementary material Fig. S4); and two fell into a category we termed 'Other' (supplementary material Fig. S4). These 52 lines were also crossed to *GMR-Gal4* alone to determine whether they disrupted eye development independently of *GMR-hid* (supplementary material Fig. S4). Because many UAS-RNAi lines caused a rough eye phenotype with *GMR-Gal4* alone and thus may disrupt eye development in a process distinct from CP, we performed a secondary screen to assess CP within the larval eye discs (Fig. 2D). In many of the 52 RNAi lines tested, we observed normal or slightly disrupted CP (supplementary material Fig. S4). Four RNAi lines caused a striking loss of CP: *Dp*, *scalloped* (*sd*), *fork head* and *knirps*. *Dp* is known to be required for entry into S phase (Frolov et al., 2005) and thus was not characterized further. Of the remaining three genes, we focused our studies on Sd, a TEAD/TEF transcription factor that regulates growth and apoptosis in many developing tissues (Simmonds et al., 1998; Goulev et al., 2008; Wu et al., 2008; Zhang et al., 2008).

Scalloped is required for compensatory proliferation

CP is substantially reduced in *GMR-hid* discs by *sd* knockdown with either of two independently derived RNAi lines (Fig. 3A,B,G). To verify this result, we tested whether a *sd* mutation would also block CP. Because *sd* null mutants are embryonic lethal (Deshpande et al., 1997), we generated *sd* mutant clones in *GMR-hid* eye discs using the *ey>FLP/FRT* system (Fig. 3C-C‴). Whereas wild-type clones contain EdU-positive cells in the position of the CP wave, *sd* mutant clones do not (Fig. 3C″,C‴). Although apoptosis is slightly decreased in *GMR>hid, sd RNAi* discs compared with *GMR>hid, luc RNAi* (Fig. 3A,B,H), the decrease in CP is not due to the decrease in apoptosis because many *GMR>hid, sd RNAi* discs have the same amount of apoptosis as controls, whereas none has the same degree of CP as controls (Fig. 3H). Taken together, these results indicate that Sd is a CP regulator.

Recent results suggest that in certain contexts Sd can act as a suppressor of genes controlling apoptosis and growth. This

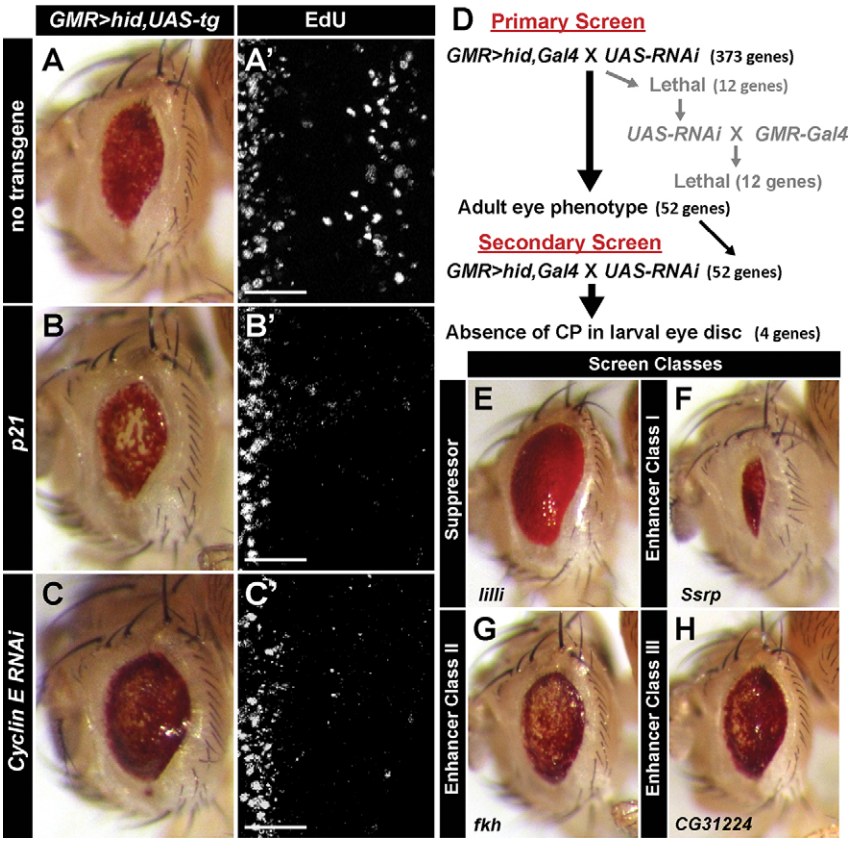

Fig. 2. Genetic screen for regulators of compensatory proliferation. (A-C′) Adult eyes (A-C) and high magnification view of posterior eye imaginal discs (A′-C′; as in Fig. 1B′) expressing the indicated UAS-transgenes in *GMR-hid, GMR-Gal4*/+ individuals. (D) Schematic of the RNAi screen. (E-H) Representative examples of the four categories of adult eye phenotypes resulting from the RNAi screen. See also supplementary material Table S1 and Figs S3,S4. Anterior is oriented to the left. Scale bars: 20 µm.

Development (2015) 142, 2740-2751 doi:10.1242/dev.119339

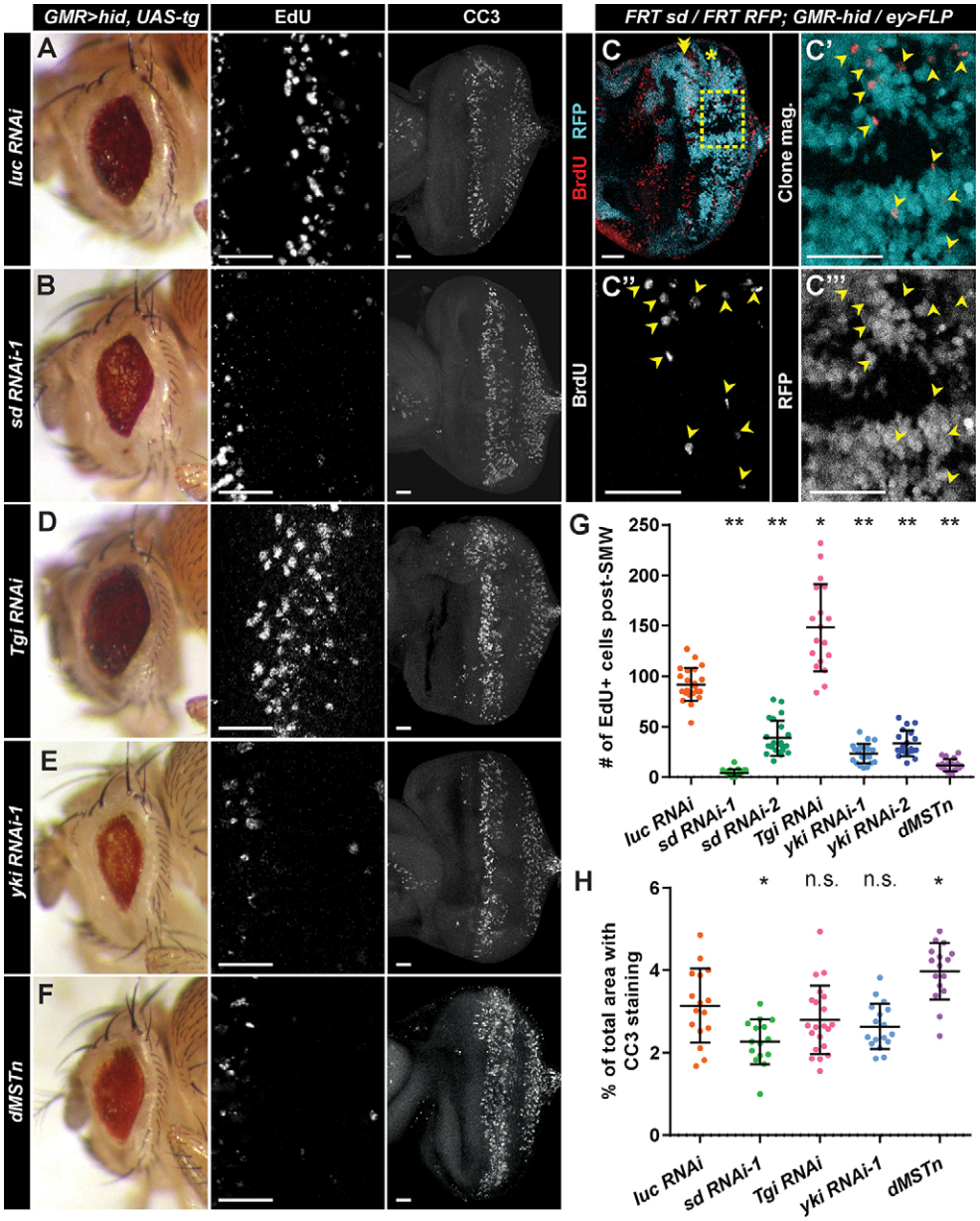

Fig. 3. *sd* and *yki* are required for compensatory proliferation. (A,B,D-F) Adult eyes (left panels), high magnification of posterior eye discs stained with EdU (middle panels), and apoptosis as detected by CC3 staining (right panels) in *GMR>hid, Gal4* discs expressing the indicated transgenes. *luciferase* (*luc*) RNAi is used as a control (A). (C-C‴) Clones of wild-type (RFP^+, cyan) and *sd* mutant (RFP^-) cells in the *GMR-hid* background. Boxed area in C indicates area of magnification shown in C′-C‴. Double arrowhead indicates SMW; asterisk indicates CP. Arrowheads indicate $BrdU^+$ cells. (G) Quantification of CP in the *GMR>hid, Gal4* background for the indicated UAS-transgenes. Each circle represents the number of cells counted for a single disc, and bars represent mean and one standard deviation. For each genotype, $n \geq 19$ discs. (H) Quantification of percentage of total disc area with CC3 staining in the *GMR>hid, Gal4* background for the indicated UAS-transgenes. Each circle represents the percentage for a single disc, and bars represent mean and one standard deviation. For each genotype, $n \geq 15$ discs. $^*P \leq 3\times10^{-3}$, $^{**}P \leq 3\times10^{-13}$. n.s., not significant. Anterior is oriented to the left. Scale bars: 20 µm.

suppressor activity is dependent on the Tondu-domain-containing Growth Inhibitor (Tgi) co-factor (Koontz et al., 2013). We reasoned that the slight decrease in apoptosis in *GMR>hid, sd RNAi* discs could reflect Sd suppressor activity. However, the amount of apoptosis is unchanged in *GMR>hid, Tgi RNAi* discs relative to control (Fig. 3D,H). Interestingly, CP increases in *GMR>hid, Tgi RNAi* discs (Fig. 3D,G), possibly as a result of increased growth gene expression (Fig. 3D). The opposing phenotypes of *sd* and *Tgi* RNAi in the *GMR-hid* background make it unlikely that Sd is acting as a suppressor to induce CP.

Yorkie is required for compensatory proliferation

Sd activates expression of target genes in the eye disc as part of a complex with Yorkie (Yki), the transcriptional effector of the Hippo pathway (Goulev et al., 2008; Wu et al., 2008; Zhang et al., 2008). The Hippo pathway controls tissue growth by regulation of Yki, targets of which include cell cycle regulators, such as *Cyclin E* (Huang et al., 2005) and *E2f1* (Goulev et al., 2008), and anti-apoptotic genes, such as *Diap1* (Huang et al., 2005) and *ban* (Thompson and Cohen, 2006). Flux through the Hippo pathway is governed by Hippo (Hpo) phosphorylation of Warts (Wts), which in turn phosphorylates Yki. Phosphorylated Yki cannot translocate to the nucleus (Oh and Irvine, 2008). Thus, increased Hippo signaling reduces transcription of Yki target genes. Unphosphorylated, nuclear Yki acts as a co-activator for transcription factors, such as Sd and the Homothorax (Hth)/Teashirt (Tsh) complex (Peng et al., 2009). Because Yki itself does not bind DNA, it was not included in our initial screen. Targeting *yki* with two independently derived UAS-RNAi transgenes reduced CP and resulted in an adult eye phenotype similar to *sd* RNAi (Fig. 3E,G). Levels of apoptosis in *GMR>hid, yki RNAi* discs were not significantly different from controls (Fig. 3H). We further probed the contribution of Yki to CP by overexpressing the Hpo kinase domain (dMSTn; Zhang et al., 2008), which blocks Yki activity. The adult eye phenotypes were similar to those elicited by *sd* or *yki* RNAi (Fig. 3F), and CP in the eye disc was significantly reduced compared with controls

Development (2015) 142, 2740-2751 doi:10.1242/dev.119339

(Fig. 3F,G). We conclude that Yki is necessary to induce CP in eye discs, suggesting a shared role for Hippo signaling in regulating CP in eye and wing discs.

Cyclin E is induced by Sd/Yki during compensatory proliferation

Sd/Yki targets include *Cyclin E*, *Diap1*, *expanded* (*ex*) and *ban* (Wu et al., 2008; Zhang et al., 2008). As Cyclin E is required for CP (Fig. 2C), we compared Cyclin E levels in wild-type and *GMR-hid* discs. In proliferating cells, like those anterior to the MF or within the SMW, Cyclin E levels rise during G1 to induce entry into S phase (Fig. 4A) (Knoblich et al., 1994), then fall during S phase and mitosis as a result of transcriptional (Duronio and O'Farrell, 1995) and post-translational (Moberg et al., 2001) regulation. In wild-type eye discs, Cyclin E levels are low in quiescent cells posterior to the SMW (Fig. 4B) (Richardson et al., 1995). By contrast, Cyclin E expression is high posterior to the SMW in *GMR-hid* and *GMR>hid, luc RNAi* discs (Fig. 4C,D). This increase in Cyclin E accumulation occurred primarily in Yan^{+} undifferentiated cells rather than in photoreceptors (Fig. 4C,D). *sd* or *yki* RNAi reduces Cyclin E accumulation posterior to the SMW (Fig. 4E-G). These data suggest that Sd/Yki induce Cyclin E

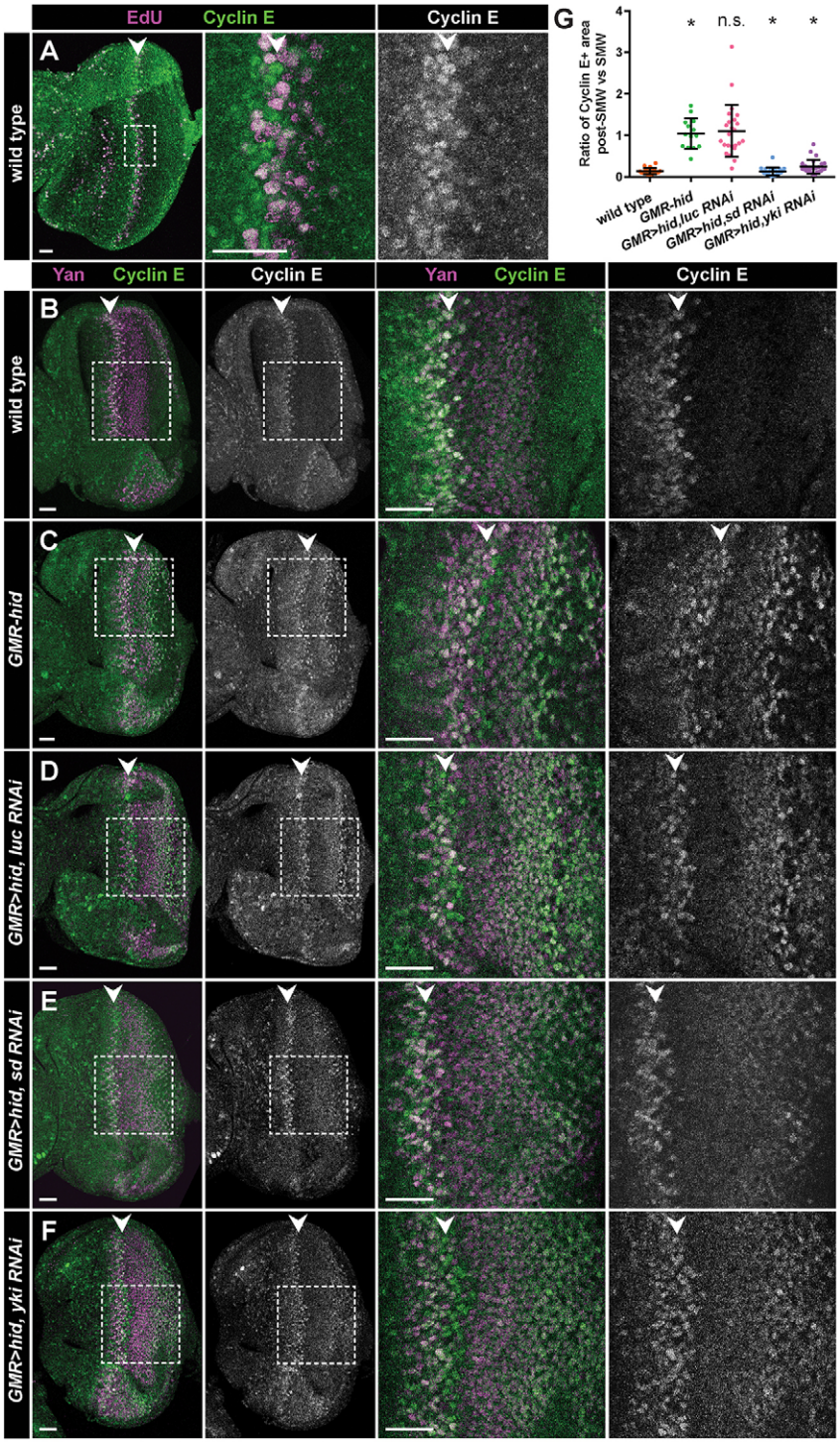

Fig. 4. Sd and Yki are required for elevated Cyclin E levels during CP. (A) Eye disc labeled with EdU (magenta) and anti-Cyclin E (green) antibodies. Cyclin E accumulates prior to and during S phase of the SMW (arrowhead). Box in left panel indicates area of magnification in middle and right panels. (B-F) Eye discs of the indicated genotypes stained with anti-Cyclin E (green) and anti-Yan (marker of undifferentiated cells; magenta) antibodies. Boxes indicate areas shown at higher magnification on the right. Arrowheads indicate SMW. (G) Quantification of Cyclin E staining in Yan^{+} cells of the indicated genotypes. The ratio of post-SMW Cyclin E staining versus SMW Cyclin E staining is displayed (see supplementary Methods for details). Each circle represents the ratio calculated for a single disc, and bars represent mean and one standard deviation. For each genotype, $n \geq 14$ discs. *$P \leq 1.8\times10^{-7}$. Significance was calculated for wild type (w^{1118}) versus *GMR-hid*, *GMR-hid* versus *GMR>hid, luc RNAi*, *GMR>hid, luc RNAi* versus *GMR>hid, sd RNAi*, and *GMR>hid, luc RNAi* versus *GMR>hid, yki RNAi*. n.s., not significant. Anterior is oriented to the left. Scale bars: 20 µm.

Development (2015) 142, 2740-2751 doi:10.1242/dev.119339

expression in regenerating eye discs, driving S-phase entry during CP.

We next examined expression of the Yki targets *ex* and *ban* in *GMR-hid* tissues. Whereas we observe CP (supplementary material Fig. S5A) and apoptosis (supplementary material Fig. S5B) in *GMR-hid* clones, we do not observe differences in expression of a transgene that detects *ban* activity (Brennecke et al., 2003) (supplementary material Fig. S5C) or *ex-lacZ* expression (supplementary material Fig. S5D) between wild-type and *GMR-hid* clones. Additionally, we do not observe an increase in *ban* sensor expression or *ex-lacZ* in *GMR-hid* discs compared with wild-type discs (supplementary material Fig. S5E,F).

Yki overexpression rescues *GMR-hid* phenotypes

Because Yki overexpression induces *Cyclin E* expression and proliferation (Huang et al., 2005), we tested whether increased Yki expression rescues *GMR-hid* phenotypes. We utilized both wild-type Yki and a version of Yki (Yki^{S168A}) that is hyperactive owing to reduced phosphorylation by Wts (Oh and Irvine, 2008). *GMR-Gal4*-driven expression of either Yki or Yki^{S168A} induces Cyclin E and ectopic S-phase entry, but not apoptosis, posterior to the MF (supplementary material Fig. S6). Yki^{S168A} expression induces a considerable number of cells to enter S phase, resulting in extensive overgrowth in both the larval disc (supplementary material Fig. S6B″) and the adult eye (supplementary material Fig. S6A″). Similar results were obtained in the *GMR>hid, Gal4* background (Fig. 5). Both Yki and Yki^{S168A} expression result in high Cyclin E accumulation throughout the posterior of *GMR>hid, Gal4* discs (Fig. 5C-C″). Although the adult eye morphology, CP and apoptosis appear similar in control and *GMR>hid, yki* discs (Fig. 5A′,B′,D′), there is an increase of cells in S phase in *GMR>hid,* yki^{S168A} discs (Fig. 5B″), and overgrowth occurs in both the disc and the adult eye (Fig. 5A″,B″). Therefore, overexpression of Yki^{S168A} rescues the small eye phenotype caused by *GMR-hid*, indicating that Yki activation is sufficient to overcome cell loss after Hid induction.

Although suppression of the *GMR>hid, Gal4* eye phenotype by Yki^{S168A} expression is likely to be due primarily to extensive over-proliferation, we also measured apoptosis in this genotype. Apoptosis is significantly decreased in *GMR>hid,* yki^{S168A} discs, particularly in the second apoptotic wave (Fig. 5D″,G). As *Diap1* is a Yki target and suppressor of apoptosis, we measured *Diap1-lacZ* levels after Hid and Yki^{S168A} expression. *Diap1-lacZ* levels posterior to the furrow increase after Hid expression and increase further with Hid and Yki^{S168A} expression (Fig. 5E,F). Thus, Yki-dependent *Diap1* expression may play a role in limiting cell death after *hid* induction. Although apoptosis is not increased in *GMR>hid, yki RNAi* discs, apoptosis is increased in *GMR>hid, dMSTn* discs (Fig. 3F,H). *GMR>hpo* discs also display moderate apoptosis, independently of Hid expression (Verghese et al., 2012). These data suggest that in addition to its role in CP, Yki activity can regulate apoptosis during tissue damage.

Our data suggest that Yki activation is a key step in CP initiation. We therefore hypothesized that Yki activity is limiting for entry into S phase during CP. If true, an increase in Yki posterior to the MF would sensitize cells to CP signals, resulting in earlier S-phase entry that would manifest in a shift of the CP wave towards the anterior. Indeed, the distance between the anterior border of the SMW and the anterior border of the compensatory wave in *GMR>hid, yki* discs is decreased compared with *GMR>hid, luc RNAi* (Fig. 5B,H). Because distance along the anteroposterior axis of the eye disc is a proxy for time, these data indicate that cells re-enter S phase sooner in *GMR-hid* discs expressing additional Yki compared with those without. These data suggest that levels of Yki are important for controlling CP timing and that active Yki may be the limiting factor for inducing cell cycle re-entry.

Ajuba, an inhibitor of Hippo signaling, is required for compensatory proliferation

How is Hippo signaling inhibited to allow Yki activation during tissue regeneration? Flux through the Hippo pathway is modulated by events at the cell cortex that monitor epithelial integrity and cell-cell interaction (Yu and Guan, 2013). One mechanism for inhibiting Hippo signaling is through the LIM domain protein Ajuba (Jub). Jub antagonizes Hippo signaling and is essential for eye development (Das Thakur et al., 2010). Activated Jub is thought to inhibit Hippo signaling by binding Wts, thereby preventing Wts from phosphorylating Yki (Rauskolb et al., 2014). *jub* RNAi enhances the *GMR>hid, Gal4* adult eye phenotype and reduces CP (Fig. 6A,B,L). This observation is consistent with observations in the wing disc where reduced Jub inhibits regeneration (Sun and Irvine, 2013). Jub localizes with DE-cadherin (Shotgun – FlyBase) at apical adherens junctions in larval eye discs (Fig. 6C), as in pupal eye discs (Das Thakur et al., 2010) and wing discs (Sun and Irvine, 2013). This localization is most apparent at the apical surface of photoreceptors (Fig. 6D). We did not observe obvious accumulation or re-localization of Jub in *GMR-hid* clones (Fig. 6E), suggesting that increased activation rather than re-localization of Jub may be required to inhibit Hippo signaling during CP.

Jub can be activated in wing discs by JNK signaling (Sun and Irvine, 2013) or by an increase in cellular tension (Rauskolb et al., 2014). Because our data suggest that JNK signaling does not play a significant role in CP in the eye disc (supplementary material Fig. S2B-G), we investigated whether increased cellular tension modulates CP. We induced an increase in cellular tension by expressing the catalytic domain of Rho kinase (RokCAT), which phosphorylates myosin and leads to increases in myosin contractility (Winter et al., 2001). In *GMR>hid, RokCAT* discs, CP increases by twofold, although the adult eye phenotype is not noticeably altered (Fig. 6F,L). Conversely, *Rok* RNAi results in a mild but statistically significant decrease in CP (Fig. 6L). Rok is activated by the Rho1 GTPase (Warner et al., 2010), which is inhibited in the pupal retina by Cdc42 (Warner and Longmore, 2009). Cdc42 also inhibits CP in irradiated wing discs (Warner et al., 2010). We observed an increase in CP in *GMR-hid* discs with expression of dominant-negative Cdc42 ($Cdc42^{DN}$) (Fig. 6I,L). These results suggest that regulation of cellular tension through Cdc42/Rho/Rok plays a role in CP, presumably through Jub regulation.

We predicted that increases in cellular tension in the absence of Hid expression would also activate Jub and induce cell cycle re-entry. Indeed, when RokCAT was expressed with *GMR-Gal4* alone, we observed ectopic S phases in the posterior of the disc (Fig. 6G,L). We also observed a low level of apoptosis in *GMR>RokCAT* eye discs (Fig. 6G), similar to previous results in wing discs (Warner et al., 2010). We investigated whether the cell cycle entry in the posterior of *GMR>RokCAT* discs depends on the presence of these apoptotic cells by labeling *GMR>RokCAT, p35* eye discs with EdU and anti-CC3 antibodies. p35 blocks RokCAT-induced apoptosis, which we confirmed by the lack of basally extruded cells and pyknotic nuclei, but does not block CC3 staining owing to the presence of non-cleaved-caspase epitopes of the anti-CC3 antibodies in undead cells (Fan and Bergmann, 2010). Suppression of apoptosis in *GMR>RokCAT, p35* discs did not prevent the appearance of ectopic EdU-positive

Development (2015) 142, 2740-2751 doi:10.1242/dev.119339

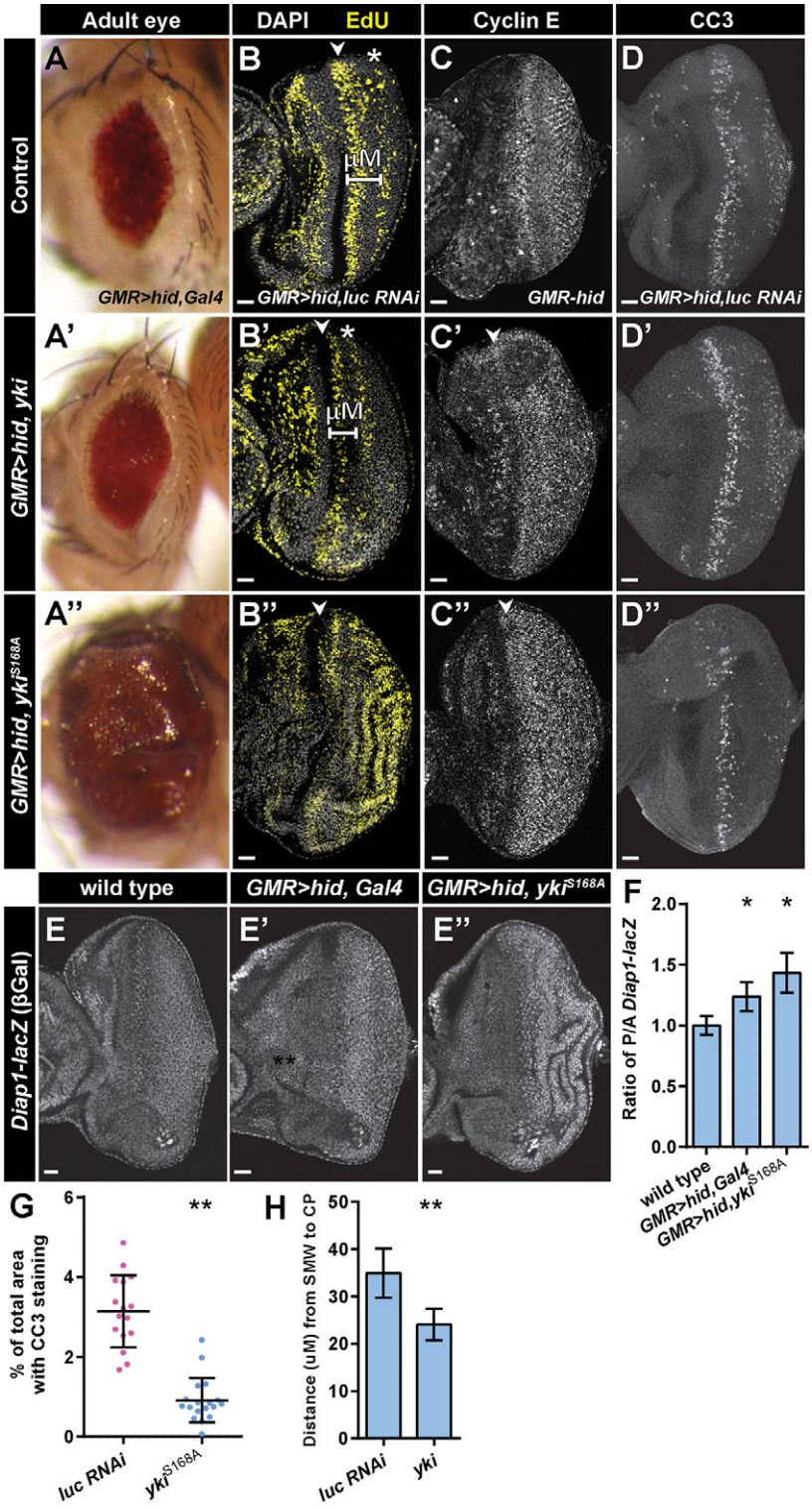

Fig. 5. Expression of transgenic *yki* modifies the *GMR-hid* phenotype. (A-A″) *GMR>hid, Gal4* adult eyes (control in A) after expression of *yki* (A′) or yki^{S168A} (A″). (B-B″) EdU staining (yellow) in eye discs of the indicated genotypes. Arrowheads indicate SMW. The white bar (B,B′) indicates the distance measured between the SMW and CP (asterisk) (data shown in H). (C-C″) Cyclin E staining of the indicated genotypes. (D-D″) CC3 staining of the indicated genotypes. (E-E″) β-Gal staining of the indicated genotypes detects *Diap1-lacZ* expression. (F) Quantification of *Diap1-lacZ* expression by β-Gal staining [ratio of posterior to anterior (P/A) eye disc, normalized to w^{1118} control] in the indicated genotypes. Error bars represent one standard deviation. $*P \leq 6\times10^{-4}$, $n \geq 11$ discs. (G) Quantification of percentage of total disc area with post-furrow CC3 staining in *GMR>hid, Gal4* eye discs expressing *luc RNAi* (n=16) or yki^{S168A} (n=18). Each circle represents the percentage calculated for a single disc, and bars represent mean and one standard deviation. $**P=3.64\times10^{-6}$. (H) Quantification of the distance between the SMW and CP wave in *GMR>hid, Gal4* eye discs expressing *luc RNAi* (n=25) or *yki RNAi* (n=22). $**P=8.47\times10^{-11}$. Error bars represent one standard deviation. Anterior is oriented to the left. Scale bars: 20 μm.

cells posterior to the SMW, indicating that RokCAT directly induces S-phase entry (Fig. 6H,L). We also observed cell cycle re-entry in *GMR>Cdc42*^{DN} discs, even when p35 was co-expressed (Fig. 6J-L). In wing discs, co-expression of RokCAT and p35 induces hyperproliferation (Warner et al., 2010), which could be attributed to the formation of undead cells rather than increases in tension directly inducing proliferation. However, as p35 expression blocks CP in post-furrow eye discs and does not induce mitogenic undead cells (Fan and Bergmann, 2008), our results suggest that modulation of cellular tension directly induces cell cycle re-entry posterior to the SMW.

DISCUSSION

To maintain tissue homeostasis and prevent inappropriate cell divisions, the threshold for S-phase entry is higher in quiescent cells than in cycling cells. Consequently, to undergo regeneration efficiently, quiescent tissues must overcome robust controls that restrain cell cycle entry. The mechanisms that drive cell cycle

Development (2015) 142, 2740-2751 doi:10.1242/dev.119339

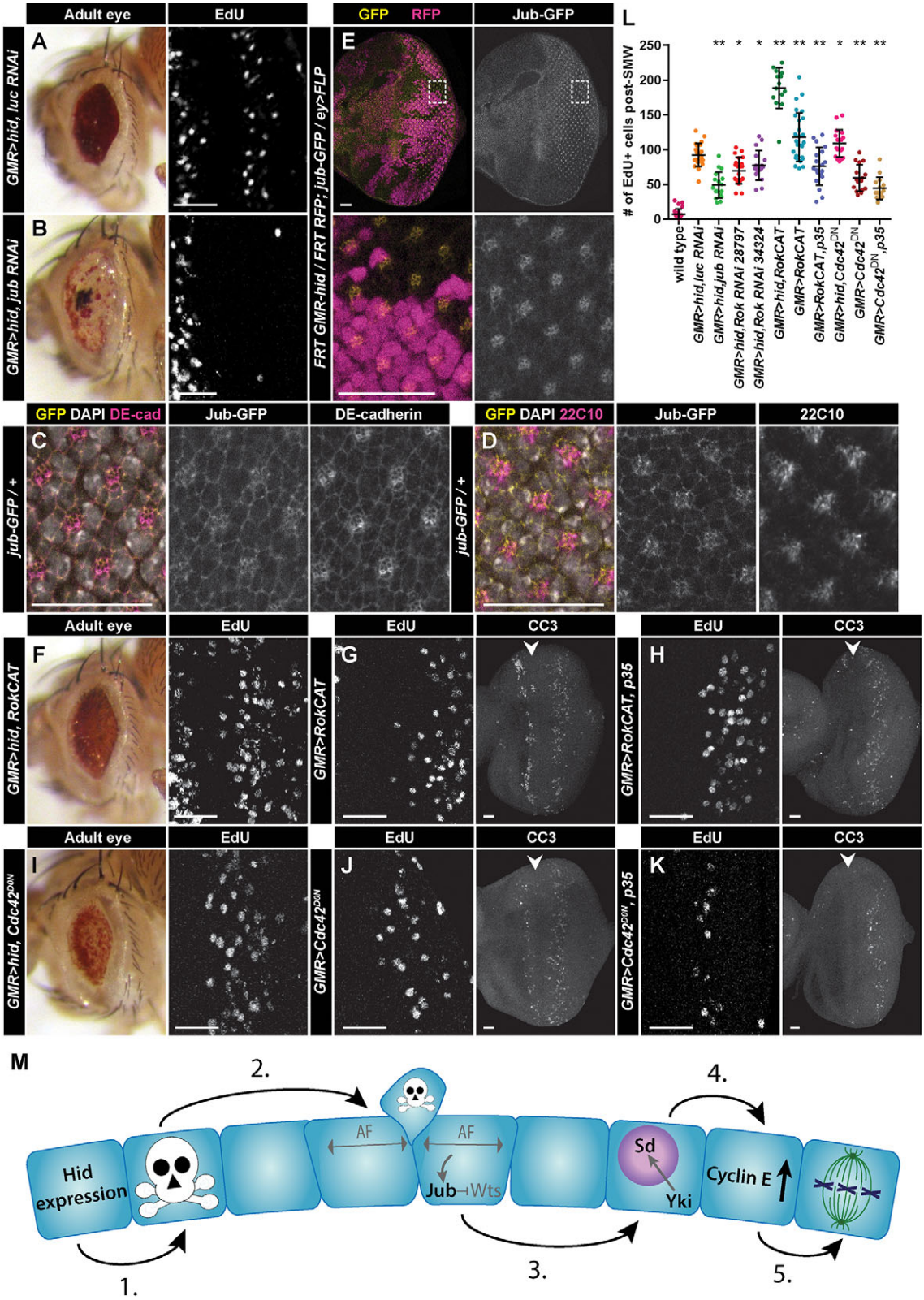

Fig. 6. See next page for legend.

re-entry and regeneration in a quiescent cell population are largely unknown, in part because many studies of regeneration have been performed in proliferative tissues. Here, we report the results from a genetic screen identifying regulators of tissue damage-induced cell cycle re-entry of a quiescent cell population in *Drosophila*.

Scalloped and Yorkie regulate compensatory proliferation in eye imaginal discs

We found that Sd and Yki are required for quiescent cells in the eye imaginal disc to enter the cell cycle in response to tissue damage. Specifically, Sd and Yki are required for Cyclin E accumulation

Development (2015) 142, 2740-2751 doi:10.1242/dev.119339

Fig. 6. Jub and cellular tension regulate compensatory proliferation. (A,B,F,I) Adult eyes (left panels) and high magnification of post-furrow EdU staining (right panels) of the indicated genotypes. (C,D) Jub-GFP (yellow) colocalizes with DE-cadherin (magenta; C) and Futsch/22C10, a marker of neuronal membranes (magenta; D), at the apical surface of post-furrow eye discs. (E) Clones of *GMR-hid* (no marker) and wild-type (RFP^+, magenta) cells expressing Jub-GFP (yellow). Boxes in top panels indicate area of magnification shown in bottom panels. (G,H,J,K) High magnification of post-furrow EdU staining (left panels) and CC3 staining (right panels) of the indicated genotypes. Arrowheads mark the MF. *GMR>RokCAT* (G) and *GMR>Cdc42^{DN}* (J) induce CC3-positive apoptotic cells posterior to the MF. Interestingly, apoptotic cells are also observed anterior to the furrow in these discs. The mechanism triggering this apoptosis is unknown, but its absence in *GMR>RokCAT, p35* (H) or *GMR>Cdc42^{DN}, p35* (K) discs suggests the anterior induction of apoptosis in *GMR>RokCAT* and *GMR>Cdc42^{DN}* discs is dependent on apoptosis posterior to the furrow. CC3 staining persists posterior to the furrow after p35 expression (H,K) because undead cells express non-cleaved-caspase epitopes of the anti-CC3 antibodies (Fan and Bergmann, 2010). (L) Quantification of CP in the indicated genotypes. *GMR>hid, Gal4* genotypes were compared with *GMR>hid, luc RNAi*, whereas *GMR>Gal4* genotypes were compared with wild type (w^{1118}). Each circle represents the number of cells counted for a single disc, and bars represent mean and one standard deviation. For each genotype, $n \geq 14$ discs. $^*P \leq 0.02$, $^{**}P \leq 1\times10^{-7}$. (M) Model for induction of CP in a quiescent epithelium. Text in gray indicates proposed possibilities that have not formally been observed in this study. (1) Hid expression/tissue damage induces apoptosis in a subset of cells. (2) Basal extrusion of apoptotic cells induces apoptotic force (AF), which activates Jub, leading to Wts inhibition. (3) Wts inhibition results in Yki translocating to the nucleus and acting as a transcriptional co-activator for Sd. (4) Sd/Yki induce high levels of Cyclin E, which induces cell cycle re-entry (5). Anterior is oriented to the left. Scale bars: 20 µm.

following damage, presumably through transcriptional control of *Cyclin E*. Initial experiments suggested that Yki and Sd act together to drive gene transcription, as Sd is required for overgrowth and target gene induction following Yki overexpression in the eye disc (Wu et al., 2008; Zhang et al., 2008). However, their roles during eye development are clearly distinct as *yki* mutant clones grow poorly in the eye disc (Huang et al., 2005) whereas *sd* mutant clones grow normally (Zhang et al., 2008). In addition, Sd and Yki have both overlapping and unique binding sites throughout the genome, many of which are tissue dependent (Slattery et al., 2013). Curiously, mutation of *sd* rescues growth defects in *yki* mutant clones, suggesting that Yki may relieve Sd-mediated gene repression (Koontz et al., 2013). Additional factors, such as Tgi, probably function as co-factors for Sd suppressor function (Koontz et al., 2013). Conversely, Sd/Yki may act synergistically with E2f1 (Nicolay et al., 2011) and GAGA factor (Trithorax-like – FlyBase) (Bayarmagnai et al., 2012; Oh et al., 2013) to drive gene expression. Although our data suggest that Sd activates transcription during CP, it will be important to determine how Sd/Yki co-factors are regulated during development and tissue damage to allow robust Sd/Yki target gene expression.

Cyclin/Cdk regulation is a conserved mechanism for inducing regeneration

Cyclin/Cdk regulation is essential for regeneration in many model organisms. In post-mitotic *Caenorhabditis elegans* muscle cells, ectopic expression of cyclins drives DNA replication and cell division (Korzelius et al., 2011). Mice mutant for the CDK inhibitor p21 (Cdkn1a – Mouse Genome Informatics) robustly regenerate lost skin in the ear, which normally does not regenerate (Bedelbaeva et al., 2010). This suggests that regulation of Cyclin/Cdk activity may confer regenerative capabilities on otherwise non-regenerative tissues.

Previous work has shown that high levels of cell cycle regulators are required drive cell cycle re-entry in post-mitotic cells (Buttitta et al., 2007). The G1-S transition is driven by a positive feedback loop between E2f1 and Cyclin E where E2f1 induces *Cyclin E* transcription, and Cyclin E/Cdk2 inhibits Rbf, the E2f1 inhibitor. In post-mitotic photoreceptors, high levels of Rbf and Dacapo keep E2f1 and Cyclin E/Cdk2 in check, and activation of both E2f1 and Cyclin E/Cdk2 is necessary to overcome cell cycle exit (Buttitta et al., 2007). In quiescent, undifferentiated cells of the developing eye disc, high levels of ectopic Cyclin E are sufficient to overcome cell cycle arrest and drive S-phase entry (Richardson et al., 1995). Undifferentiated eye disc cells may be poised to respond to damage-induced Cyclin E expression.

Although our results suggest that Sd/Yki induce Cyclin E accumulation during CP, there are likely to be other inputs that drive cell cycle re-entry. The Hedgehog pathway transcription factor Ci, which is required for CP in the post-furrow eye (Fan and Bergmann, 2008), can directly activate *Cyclin E* transcription in the eye disc (Duman-Scheel et al., 2002). Yki and Ci also have other cell cycle targets: Yki can activate *E2f1* transcription in the wing disc (Goulev et al., 2008) and Ci induces *Cyclin D* expression in the eye disc (Duman-Scheel et al., 2002). We postulate that a combination of Ci and Sd/Yki activity drives a *Cyclin E*-containing gene expression program that induces cell cycle entry and CP.

Apoptotic force may link cell death to Yki activation

In the wing imaginal disc, Yki activity during CP is driven by Jub-dependent inhibition of Hippo signaling (Sun and Irvine, 2013). Our data indicate that Jub is also required for CP in the eye, suggesting a shared mechanism for Yki activation between tissues. However, although Jub-dependent inhibition of Hippo signaling in the wing disc requires JNK signaling, we did not find a requirement for JNK signaling for CP in the eye disc. An alternative mechanism for inhibition of the Hippo pathway is tension-induced activation of Jub (Rauskolb et al., 2014). Mechanical force has also been shown to regulate activity of the mammalian Yorkie homolog Yes-associated protein (YAP) (Aragona et al., 2013) and induce cell proliferation in culture (Streichan et al., 2014). We show that expression of Rok or dominant-negative Cdc42, which can increase cellular tension, increases cell cycle re-entry, and we propose that cellular tension in the eye disc epithelium modulates CP.

One possible source of increased cellular tension in *GMR-hid* discs is from 'apoptotic force' generated by extrusion of dying cells. The phenomenon of apoptotic force has been described in *Drosophila* embryos, in which actin/myosin-driven constriction of dying amnioserosa cells exerts force on overlying epithelial cells to drive dorsal closure (Toyama et al., 2008). Apoptotic force in *GMR-hid* discs may increase cellular tension and drive Jub activation. Several observations are consistent with a model that physical extrusion of apoptotic cells is required to generate the force necessary to induce CP. *LGMR-hid*, which induces less apoptosis than does *GMR-hid* and presumably less apoptotic force, does not induce CP. Additionally, the apoptotic-inhibitor p35, which blocks basal extrusion of apoptotic cells, inhibits CP in the eye disc posterior to the MF (Fan and Bergmann, 2008). Finally, *GMR-hid* clones exhibit S-phase entry in cells within and immediately bordering the clone (supplementary material Fig. S5; Fan and Bergmann, 2008). This observation suggests that CP could result from local changes in tension rather than a long-range signal.

Conclusions

The Hippo pathway is a well-conserved regulator of tissue growth and is modulated in processes such as regeneration and tumor growth. YAP is required for intestinal regeneration in mice

Development (2015) 142, 2740-2751 doi:10.1242/dev.119339

(Cai et al., 2010) and confers regenerative ability in normally non-regenerative mouse hearts (Xin et al., 2013). Importantly, tight control of the Hippo pathway is crucial for tissue homeostasis, as YAP hyperactivity or inhibition of the Hippo pathway promotes cancer in many contexts (Johnson and Halder, 2014). Therefore, knowledge gained from studies of CP in *Drosophila* imaginal discs will contribute to understanding the role of Hippo signaling in mammalian regeneration and cancer.

MATERIALS AND METHODS

Mutants and transgenes

Wild-type control is w^{1118} unless otherwise noted. All adult eye images are from females. Fly stocks were obtained from the Bloomington Stock Center or from colleagues (see supplementary Methods for more details), with the exception of *LGMR-hid* (construction described in the supplementary Methods). All lines used for the RNAi screen are from the Transgenic RNAi Project (TRiP) at Harvard Medical School, with details provided in supplementary material Table S1.

Immunostaining

Eye discs were dissected from wandering third instar larvae. Discs were incubated with 100 µg/ml 5-ethynyl-2′-deoxyuridine (EdU) or 1 mg/ml 5-bromo-2′-deoxyuridine (BrdU) for 60 min and fixed for 20 min with 4% formaldehyde. EdU detection was performed with the Click-iT EdU Alexa Fluor 555 kit (Molecular Probes) according to the manufacturer's protocol. Antibodies used are as follows: rabbit anti-cleaved Caspase-3 (1:200; 9661, Cell Signaling), rat anti-Elav [1:100; 7E8A10, Developmental Studies Hybridoma Bank (DSHB)], mouse anti-βGal (1:1000; 40-1a, DSHB), mouse anti-Cyclin E (1:200; 8B10, a gift from H. Richardson, The Peter MacCallum Cancer Centre, Melbourne, Australia), mouse anti-Yan (1:500; 8B12H9, DSHB), rat anti-DE-cadherin (1:1000; DCAD2, DSHB), mouse anti-Futsch/22C10 (1:1000; DSHB), mouse anti-BrdU (1:200; B44, BD Biosciences), Alexa 488-conjugated goat anti-rabbit (1:500; 111-545-144, Jackson ImmunoResearch), Cy5-conjugated donkey anti-rat (1:500; 712-175-153, Jackson ImmunoResearch). For CC3 staining, discs were incubated with primary antibodies for 48 h at 4°C in PBS and a 2 h PBS-0.1%Triton X-100; 5% normal goat serum block was performed prior to applying secondary antibodies. Fluorescence *in situ* hybridizations were performed as previously described (Tomancak et al., 2002) with the following modifications: RNA probe was generated by T7 polymerase *in vitro* transcription in the presence of digoxigenin-11-UTP (Roche) from linearized *hid* cDNA (clone AT13267, BDGP). Detection was performed with peroxidase-conjugated anti-DIG (1:100; Roche) and Cy5-conjugated tyramide reagent (1:50; Perkin Elmer). See supplementary Methods for details on image quantification.

Acknowledgements

We thank the TRiP at Harvard Medical School and the Bloomington *Drosophila* Stock Center (National Institutes of Health P40OD018537) for stocks used in this study. Thanks to J. Jiang, D. Pan, I. Hariharan, T. T. Su, J. Poulton and J. Pearson for reagents; M. Peifer, D. Fox and F. Conlon for assistance in preparing this manuscript; and V. Boudreau for assistance with ImageJ quantification.

Competing interests

The authors declare no competing or financial interests.

Author contributions

Experiments were conceived by J.H.M. and R.J.D. Experiments were performed and data was analyzed by J.H.M. Figures were generated by J.H.M., and the manuscript was written by J.H.M. and R.J.D.

Funding

This work was funded by the National Institutes of Health National Institute of General Medical Sciences [T32-GM007092 to J.H.M. and R01-GM057859 and R01-GM058921 to R.J.D]; and the National Institutes of Health National Institute on Aging [F31-AG044957 to J.H.M.]. Deposited in PMC for release after 12 months.

Supplementary material

Supplementary material available online at
http://dev.biologists.org/lookup/suppl/doi:10.1242/dev.119339/-/DC1

References

Aragona, M., Panciera, T., Manfrin, A., Giulitti, S., Michielin, F., Elvassore, N., Dupont, S. and Piccolo, S. (2013). A mechanical checkpoint controls multicellular growth through YAP/TAZ regulation by actin-processing factors. *Cell* **154**, 1047-1059.

Baker, N. E. and Yu, S.-Y. (2001). The EGF receptor defines domains of cell cycle progression and survival to regulate cell number in the developing Drosophila eye. *Cell* **104**, 699-708.

Bandura, J. L., Jiang, H., Nickerson, D. W. and Edgar, B. A. (2013). The molecular chaperone Hsp90 is required for cell cycle exit in Drosophila melanogaster. *PLoS Genet.* **9**, e1003835.

Bayarmagnai, B., Nicolay, B. N., Islam, A. B. M. M. K., Lopez-Bigas, N. and Frolov, M. V. (2012). Drosophila GAGA factor is required for full activation of the dE2f1-Yki/Sd transcriptional program. *Cell Cycle* **11**, 4191-4202.

Bedelbaeva, K., Snyder, A., Gourevitch, D., Clark, L., Zhang, X.-M., Leferovich, J., Cheverud, J. M., Lieberman, P. and Heber-Katz, E. (2010). Lack of p21 expression links cell cycle control and appendage regeneration in mice. *Proc. Natl. Acad. Sci. USA* **107**, 5845-5850.

Bergantinos, C., Corominas, M. and Serras, F. (2010). Cell death-induced regeneration in wing imaginal discs requires JNK signalling. *Development* **137**, 1169-1179.

Bilak, A., Uyetake, L. and Su, T. T. (2014). Dying cells protect survivors from radiation-induced cell death in Drosophila. *PLoS Genet.* **10**, e1004220.

Brennecke, J., Hipfner, D. R., Stark, A., Russell, R. B. and Cohen, S. M. (2003). bantam encodes a developmentally regulated microRNA that controls cell proliferation and regulates the proapoptotic gene hid in Drosophila. *Cell* **113**, 25-36.

Bryant, P. J. (1971). Regeneration and duplication following operations in situ on the imaginal discs of Drosophila melanogaster. *Dev. Biol.* **26**, 637-651.

Buttitta, L. A., Katzaroff, A. J., Perez, C. L., de la Cruz, A. and Edgar, B. A. (2007). A double-assurance mechanism controls cell cycle exit upon terminal differentiation in Drosophila. *Dev. Cell* **12**, 631-643.

Buttitta, L. A., Katzaroff, A. J. and Edgar, B. A. (2010). A robust cell cycle control mechanism limits E2F-induced proliferation of terminally differentiated cells in vivo. *J. Cell Biol.* **189**, 981-996.

Cai, J., Zhang, N., Zheng, Y., de Wilde, R. F., Maitra, A. and Pan, D. (2010). The Hippo signaling pathway restricts the oncogenic potential of an intestinal regeneration program. *Genes Dev.* **24**, 2383-2388.

Cai, Y., Zheng, H., Gong, W., Che, Y. and Jiang, B. (2011). The role of hedgehog signaling pathway in liver regeneration. *Hepatogastroenterology* **58**, 2071-2076.

Das Thakur, M., Feng, Y., Jagannathan, R., Seppa, M. J., Skeath, J. B. and Longmore, G. D. (2010). Ajuba LIM proteins are negative regulators of the Hippo signaling pathway. *Curr. Biol.* **20**, 657-662.

de Nooij, J. C. and Hariharan, I. K. (1995). Uncoupling cell fate determination from patterned cell division in the Drosophila eye. *Science* **270**, 983-985.

Deshpande, N., Chopra, A., Rangarajan, A., Shashidhara, L. S., Rodrigues, V. and Krishna, S. (1997). The human transcription enhancer factor-1, TEF-1, can substitute for Drosophila scalloped during wingblade development. *J. Biol. Chem.* **272**, 10664-10668.

Dominguez, M. and Casares, F. (2005). Organ specification-growth control connection: new in-sights from the Drosophila eye-antennal disc. *Dev. Dyn.* **232**, 673-684.

Duman-Scheel, M., Weng, L., Xin, S. and Du, W. (2002). Hedgehog regulates cell growth and proliferation by inducing cyclin D and cyclin E. *Nature* **417**, 299-304.

Duronio, R. J. and O'Farrell, P. H. (1995). Developmental control of the G1 to S transition in Drosophila: cyclin Eis a limiting downstream target of E2F. *Genes Dev.* **9**, 1456-1468.

Fan, Y. and Bergmann, A. (2008). Distinct mechanisms of apoptosis-induced compensatory proliferation in proliferating and differentiating tissues in the Drosophila eye. *Dev. Cell* **14**, 399-410.

Fan, Y. and Bergmann, A. (2010). The cleaved-Caspase-3 antibody is a marker of Caspase-9-like DRONC activity in Drosophila. *Cell Death Differ.* **17**, 534-539.

Fan, Y. and Bergmann, A. (2014). Multiple mechanisms modulate distinct cellular susceptibilities toward apoptosis in the developing Drosophila eye. *Dev. Cell* **30**, 48-60.

Firth, L. C. and Baker, N. E. (2005). Extracellular signals responsible for spatially regulated proliferation in the differentiating Drosophila eye. *Dev. Cell* **8**, 541-551.

Fox, D. T. and Duronio, R. J. (2013). Endoreplication and polyploidy: insights into development and disease. *Development* **140**, 3-12.

Frolov, M. V., Moon, N.-S. and Dyson, N. J. (2005). dDP is needed for normal cell proliferation. *Mol. Cell. Biol.* **25**, 3027-3039.

Gibson, M. C. and Perrimon, N. (2005). Extrusion and death of DPP/BMP-compromised epithelial cells in the developing Drosophila wing. *Science* **307**, 1785-1789.

Goulev, Y., Fauny, J. D., Gonzalez-Marti, B., Flagiello, D., Silber, J. and Zider, A. (2008). SCALLOPED interacts with YORKIE, the nuclear effector of the hippo tumor-suppressor pathway in Drosophila. *Curr. Biol.* **18**, 435-441.

Grusche, F. A., Degoutin, J. L., Richardson, H. E. and Harvey, K. F. (2011). The Salvador/Warts/Hippo pathway controls regenerative tissue growth in Drosophila melanogaster. *Dev. Biol.* **350**, 255-266.

Gutierrez-Avino, F. J., Ferres-Marco, D. and Dominguez, M. (2009). The position and function of the Notch-mediated eye growth organizer: the roles of JAK/STAT and four-jointed. *EMBO Rep.* **10**, 1051-1058.
Haynie, J. L. and Bryant, P. J. (1977). The effects of X-rays on the proliferation dynamics of cells in the wing disc of Drosophila melanogaster. *Dev. Genes Evol.* **183**, 85-100.
Huang, J., Wu, S., Barrera, J., Matthews, K. and Pan, D. (2005). The Hippo signaling pathway coordinately regulates cell proliferation and apoptosis by inactivating Yorkie, the Drosophila Homolog of YAP. *Cell* **122**, 421-434.
Huh, J. R., Guo, M. and Hay, B. A. (2004). Compensatory proliferation induced by cell death in the Drosophila wing disc requires activity of the apical cell death caspase Dronc in a nonapoptotic role. *Curr. Biol.* **14**, 1262-1266.
Johnson, R. and Halder, G. (2014). The two faces of Hippo: targeting the Hippo pathway for regenerative medicine and cancer treatment. *Nat. Rev. Drug Discov.* **13**, 63-79.
Kawakami, Y., Rodriguez Esteban, C., Raya, M., Kawakami, H., Marti, M., Dubova, I. and Izpisua Belmonte, J. C. (2006). Wnt/beta-catenin signaling regulates vertebrate limb regeneration. *Genes Dev.* **20**, 3232-3237.
Knoblich, J. A., Sauer, K., Jones, L., Richardson, H., Saint, R. and Lehner, C. F. (1994). Cyclin E controls S phase progression and its down-regulation during Drosophila embryogenesis is required for the arrest of cell proliferation. *Cell* **77**, 107-120.
Koontz, L. M., Liu-Chittenden, Y., Yin, F., Zheng, Y., Yu, J., Huang, B., Chen, Q., Wu, S. and Pan, D. (2013). The Hippo effector Yorkie controls normal tissue growth by antagonizing scalloped-mediated default repression. *Dev. Cell* **25**, 388-401.
Korzelius, J., The, I., Ruijtenberg, S., Prinsen, M. B. W., Portegijs, V., Middelkoop, T. C., Groot Koerkamp, M. J., Holstege, F. C. P., Boxem, M. and van den Heuvel, S. (2011). Caenorhabditis elegans cyclin D/CDK4 and cyclin E/CDK2 induce distinct cell cycle re-entry programs in differentiated muscle cells. *PLoS Genet.* **7**, e1002362.
Li, F., Huang, Q., Chen, J., Peng, Y., Roop, D. R., Bedford, J. S. and Li, C. Y. (2010). Apoptotic cells activate the "phoenix rising" pathway to promote wound healing and tissue regeneration. *Sci. Signal.* **3**, ra13.
Moberg, K. H., Bell, D. W., Wahrer, D. C. R., Haber, D. A. and Hariharan, I. K. (2001). Archipelago regulates Cyclin E levels in Drosophila and is mutated in human cancer cell lines. *Nature* **413**, 311-316.
Mollereau, B., Perez-Garijo, A., Bergmann, A., Miura, M., Gerlitz, O., Ryoo, H. D., Steller, H. and Morata, G. (2013). Compensatory proliferation and apoptosis-induced proliferation: a need for clarification. *Cell Death Differ.* **20**, 181.
Morgan, T. H. (1901). *Regeneration*, Vol. VII. Norwood, MA: Norwood Press.
Nicolay, B. N., Bayarmagnai, B., Islam, A. B. M. M. K., Lopez-Bigas, N. and Frolov, M. V. (2011). Cooperation between dE2F1 and Yki/Sd defines a distinct transcriptional program necessary to bypass cell cycle exit. *Genes Dev.* **25**, 323-335.
Oh, H. and Irvine, K. D. (2008). In vivo regulation of Yorkie phosphorylation and localization. *Development* **135**, 1081-1088.
Oh, H., Slattery, M., Ma, L., Crofts, A., White, K. P., Mann, R. S. and Irvine, K. D. (2013). Genome-wide association of Yorkie with chromatin and chromatin-remodeling complexes. *Cell Rep.* **3**, 309-318.
Peng, H. W., Slattery, M. and Mann, R. S. (2009). Transcription factor choice in the Hippo signaling pathway: homothorax and yorkie regulation of the microRNA bantam in the progenitor domain of the Drosophila eye imaginal disc. *Genes Dev.* **23**, 2307-2319.
Perez-Garijo, A., Martin, F. A. and Morata, G. (2004). Caspase inhibition during apoptosis causes abnormal signalling and developmental aberrations in Drosophila. *Development* **131**, 5591-5598.
Perez-Garijo, A., Martin, F. A., Struhl, G. and Morata, G. (2005). Dpp signaling and the induction of neoplastic tumors by caspase-inhibited apoptotic cells in Drosophila. *Proc. Natl. Acad. Sci. USA* **102**, 17664-17669.
Perez-Garijo, A., Fuchs, Y. and Steller, H. (2013). Apoptotic cells can induce non-autonomous apoptosis through the TNF pathway. *Elife* **2**, e01004.
Pfreundt, U., James, D. P., Tweedie, S., Wilson, D., Teichmann, S. A. and Adryan, B. (2010). FlyTF: improved annotation and enhanced functionality of the Drosophila transcription factor database. *Nucleic Acids Res.* **38**, D443-D447.
Poss, K. D., Wilson, L. G. and Keating, M. T. (2002). Heart regeneration in zebrafish. *Science* **298**, 2188-2190.
Rauskolb, C., Sun, S., Sun, G., Pan, Y. and Irvine, K. D. (2014). Cytoskeletal tension inhibits Hippo signaling through an Ajuba-Warts complex. *Cell* **158**, 143-156.
Richardson, H., Okeefe, L. V., Marty, T. and Saint, R. (1995). Ectopic cyclin E expression induces premature entry into S phase and disrupts pattern formation in the Drosophila eye imaginal disc. *Development* **121**, 3371-3379.
Ruggiero, R., Kale, A., Thomas, B. and Baker, N. E. (2012). Mitosis in neurons: Roughex and APC/C maintain cell cycle exit to prevent cytokinetic and axonal defects in Drosophila photoreceptor neurons. *PLoS Genet.* **8**, e1003049.
Ryoo, H. D., Gorenc, T. and Steller, H. (2004). Apoptotic cells can induce compensatory cell proliferation through the JNK and the Wingless signaling pathways. *Dev. Cell* **7**, 491-501.
Shen, J. and Dahmann, C. (2005). Extrusion of cells with inappropriate Dpp signaling from Drosophila wing disc epithelia. *Science* **307**, 1789-1790.
Sigal, S. H., Rajvanshi, P., Gorla, G. R., Sokhi, R. P., Saxena, R., Gebhard, D. R., Jr, Reid, L. M. and Gupta, S. (1999). Partial hepatectomy-induced polyploidy attenuates hepatocyte replication and activates cell aging events. *Am. J. Physiol.* **276**, G1260-G1272.
Simmonds, A. J., Liu, X., Soanes, K. H., Krause, H. M., Irvine, K. D. and Bell, J. B. (1998). Molecular interactions between Vestigial and Scalloped promote wing formation in Drosophila. *Genes Dev.* **12**, 3815-3820.
Slattery, M., Voutev, R., Ma, L., Nègre, N., White, K. P. and Mann, R. S. (2013). Divergent transcriptional regulatory logic at the intersection of tissue growth and developmental patterning. *PLoS Genet.* **9**, e1003753.
Streichan, S. J., Hoerner, C. R., Schneidt, T., Holzer, D. and Hufnagel, L. (2014). Spatial constraints control cell proliferation in tissues. *Proc. Natl. Acad. Sci. USA* **111**, 5586-5591.
Sun, G. and Irvine, K. D. (2011). Regulation of Hippo signaling by Jun kinase signaling during compensatory cell proliferation and regeneration, and in neoplastic tumors. *Dev. Biol.* **350**, 139-151.
Sun, G. and Irvine, K. D. (2013). Ajuba family proteins link JNK to Hippo signaling. *Sci. Signal.* **6**, ra81.
Tamori, Y. and Deng, W.-M. (2013). Tissue repair through cell competition and compensatory cellular hypertrophy in postmitotic epithelia. *Dev. Cell* **25**, 350-363.
Thompson, B. J. and Cohen, S. M. (2006). The Hippo pathway regulates the bantam microRNA to control cell proliferation and apoptosis in Drosophila. *Cell* **126**, 767-774.
Tomancak, P., Beaton, A., Weiszmann, R., Kwan, E., Shu, S., Lewis, S. E., Richards, S., Ashburner, M., Hartenstein, V., Celniker, S. E. et al. (2002). Systematic determination of patterns of gene expression during Drosophila embryogenesis. *Genome Biol.* **3**, research0088.14.
Toyama, Y., Peralta, X. G., Wells, A. R., Kiehart, D. P. and Edwards, G. S. (2008). Apoptotic force and tissue dynamics during Drosophila embryogenesis. *Science* **321**, 1683-1686.
Tseng, A.-S., Adams, D. S., Qiu, D., Koustubhan, P. and Levin, M. (2007). Apoptosis is required during early stages of tail regeneration in Xenopus laevis. *Dev. Biol.* **301**, 62-69.
Verghese, S., Bedi, S. and Kango-Singh, M. (2012). Hippo signalling controls Dronc activity to regulate organ size in Drosophila. *Cell Death Differ.* **19**, 1664-1676.
Warner, S. J. and Longmore, G. D. (2009). Cdc42 antagonizes Rho1 activity at adherens junctions to limit epithelial cell apical tension. *J. Cell. Biol.* **187**, 119-133.
Warner, S. J., Yashiro, H. and Longmore, G. D. (2010). The Cdc42/Par6/aPKC polarity complex regulates apoptosis-induced compensatory proliferation in epithelia. *Curr. Biol.* **20**, 677-686.
Wenemoser, D. and Reddien, P. W. (2010). Planarian regeneration involves distinct stem cell responses to wounds and tissue absence. *Dev. Biol.* **344**, 979-991.
Wernet, M. F., Labhart, T., Baumann, F., Mazzoni, E. O., Pichaud, F. and Desplan, C. (2003). Homothorax switches function of Drosophila photoreceptors from color to polarized light sensors. *Cell* **115**, 267-279.
Winter, C. G., Wang, B., Ballew, A., Royou, A., Karess, R., Axelrod, J. D. and Luo, L. (2001). Drosophila Rho-associated kinase (Drok) links Frizzled-mediated planar cell polarity signaling to the actin cytoskeleton. *Cell* **105**, 81-91.
Worley, M. I., Setiawan, L. and Hariharan, I. K. (2012). Regeneration and transdetermination in Drosophila imaginal discs. *Annu. Rev. Genet.* **46**, 289-310.
Wu, S., Liu, Y., Zheng, Y., Dong, J. and Pan, D. (2008). The TEAD/TEF family protein Scalloped mediates transcriptional output of the Hippo growth-regulatory pathway. *Dev. Cell* **14**, 388-398.
Wuestefeld, T., Pesic, M., Rudalska, R., Dauch, D., Longerich, T., Kang, T.-W., Yevsa, T., Heinzmann, F., Hoenicke, L., Hohmeyer, A. et al. (2013). A direct in vivo RNAi screen identifies MKK4 as a key regulator of liver regeneration. *Cell* **153**, 389-401.
Xin, M., Kim, Y., Sutherland, L. B., Murakami, M., Qi, X., McAnally, J., Porrello, E. R., Mahmoud, A. I., Tan, W., Shelton, J. M. et al. (2013). Hippo pathway effector Yap promotes cardiac regeneration. *Proc. Natl. Acad. Sci. USA* **110**, 13839-13844.
Yu, F.-X. and Guan, K.-L. (2013). The Hippo pathway: regulators and regulations. *Genes Dev.* **27**, 355-371.
Zhang, L., Ren, F., Zhang, Q., Chen, Y., Wang, B. and Jiang, J. (2008). The TEAD/TEF family of transcription factor Scalloped mediates Hippo signaling in organ size control. *Dev. Cell* **14**, 377-387.
Zhang, H.-M., Chen, H., Liu, W., Liu, H., Gong, J., Wang, H. and Guo, A.-Y. (2012). AnimalTFDB: a comprehensive animal transcription factor database. *Nucleic Acids Res.* **40**, D144-D149.

Supplementary Data

Supplementary Figures

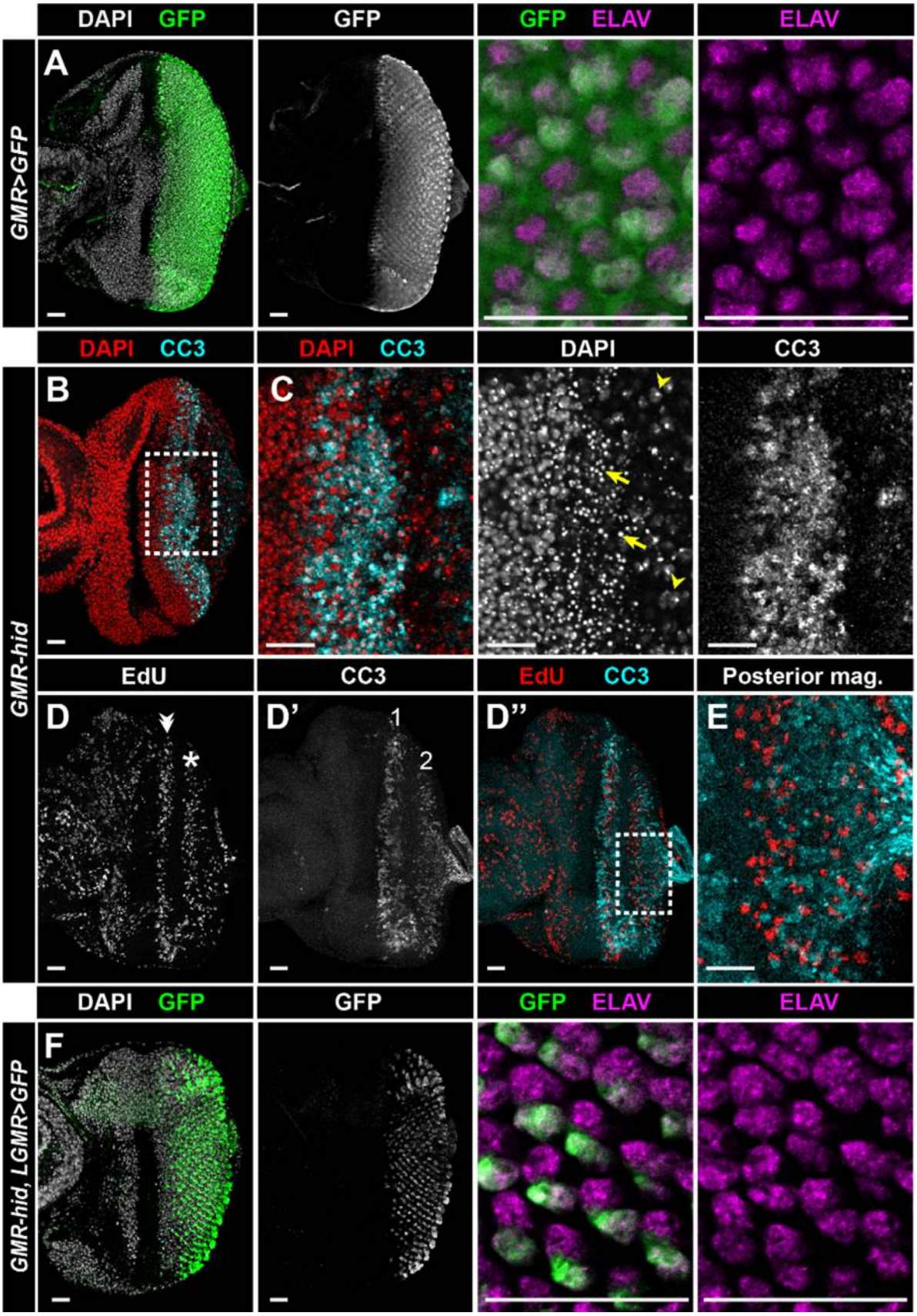

Supp. Figure 1 (related to Fig. 1). Characterization of *GMR-Gal4*, *longGMR-Gal4*, and *GMR-hid* transgenes.

A,F) Expression of GFP (green) driven by *GMR-Gal4* (A) or *longGMR-Gal4* (*LGMR-Gal4*, (F)). Higher magnification of posterior cells in the right two panels indicates photoreceptors stained with ELAV (purple). GFP is expressed in all photoreceptors with *GMR-Gal4* (A) and in a subset of photoreceptors with *LGMR-Gal4* (F).

B-C) DAPI staining of nuclei (red) and staining of apoptotic cells with anti-CC3 antibodies (cyan) on the basal surface of a *GMR-hid* disc. Box in (B) indicates area of magnification in (C). Pyknotic nuclei (arrows) and glial cell nuclei (arrowheads) are present on the basal surface of the disc.

D-E) EdU staining of cells in S-phase (red in D'') in *GMR-hid* discs marks the SMW (double arrowhead) and CP (*). CC3 staining (cyan in D'') marks the two waves of apoptosis (1 and 2). Box in D'' indicates area of magnification in E.

Anterior is oriented to the left. Scale bars: 20 μM.

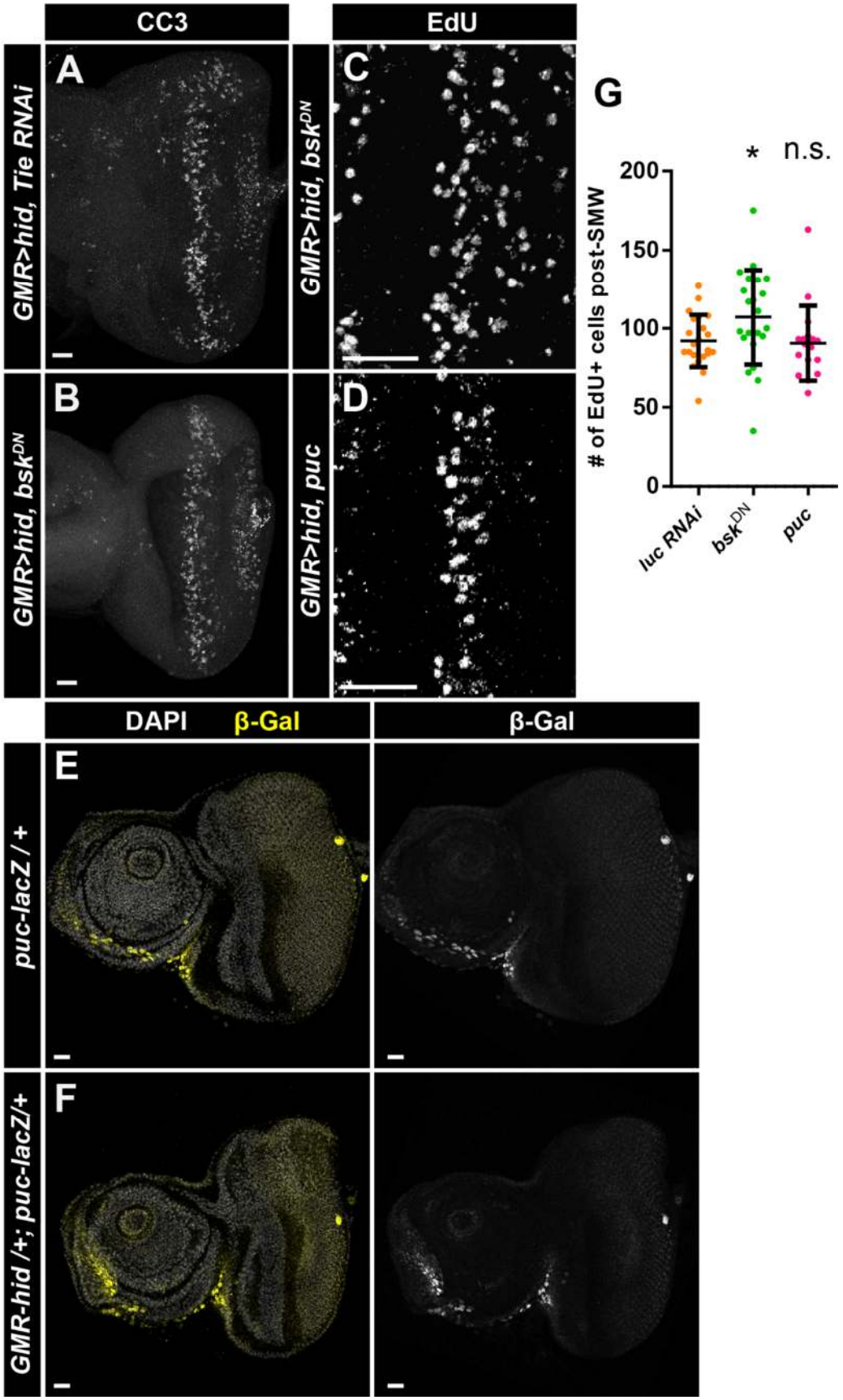
CC3
EdU
A
B
C
D
GMR>hid, Tie RNAi
GMR>hid, bskDN
GMR>hid, bskDN
GMR>hid, puc
G
* n.s.
# of EdU+ cells post-SMW
200
150
100
50
0
luc RNAi
bskDN
puc
DAPI β-Gal
β-Gal
E
F
puc-lacZ / +
GMR-hid /+; puc-lacZ/+

Supp. Figure 2 (related to Fig. 1). Inhibition of signaling through JNK or Tie does not modify the *GMR-hid* phenotype.

A,B) Apoptotic cells stained with anti-CC3 antibodies in the indicated genotypes.

C,D) EdU incorporation in the posterior of eye discs of the indicated genotypes.

E,F) *puc-lacZ* expression, marked by βGal in yellow, is similar in wild type (E) and *GMR-hid* (F) tissues.

G) Quantification of compensatory proliferating cells in the *GMR>hid,Gal4* background for the indicated UAS-transgenes. All post-SMW, EdU^+ eye disc cells were counted. Each circle on the graph represents the number of cells counted for a single disc. For each genotype, $n \geq 17$ discs. Bars represent mean and one standard deviation. n.s., not significant. While *GMR>hid, bsk^{DN}* CP is significantly increased compared to *GMR>hid, luc RNAi* (*P=0.047), it is not significantly different from another control (*GMR>hid, Gal4/CyO*; P=0.43). Therefore, we are wary about drawing conclusions about the biological significance of an increase in CP in *GMR>hid, bsk^{DN}* discs.

Anterior is oriented to the left. Scale bars: 20 μM.

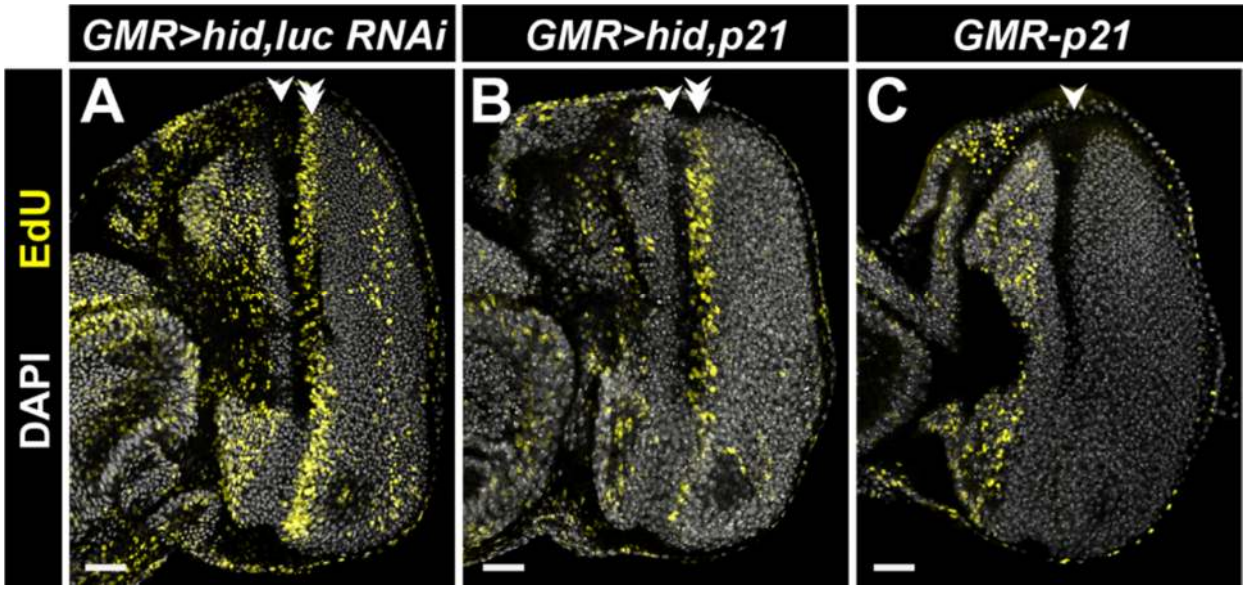

Supp. Figure 3 (related to Fig. 2). Transgenes expressed using *GMR-Gal4* do not affect the second mitotic wave.

A) *GMR>hid, luc RNAi* eye discs stained with DAPI (grey) and EdU (yellow) to indicate MF (arrowhead) and SMW (double arrowhead), respectively.

B) The SMW appears normal when *p21* is expressed with *GMR-Gal4* in the *GMR-hid* background.

C) Expressing p21 via *GMR-p21* results in ablation of the SMW.

Anterior is oriented to the left. Scale bars: 20 μM.

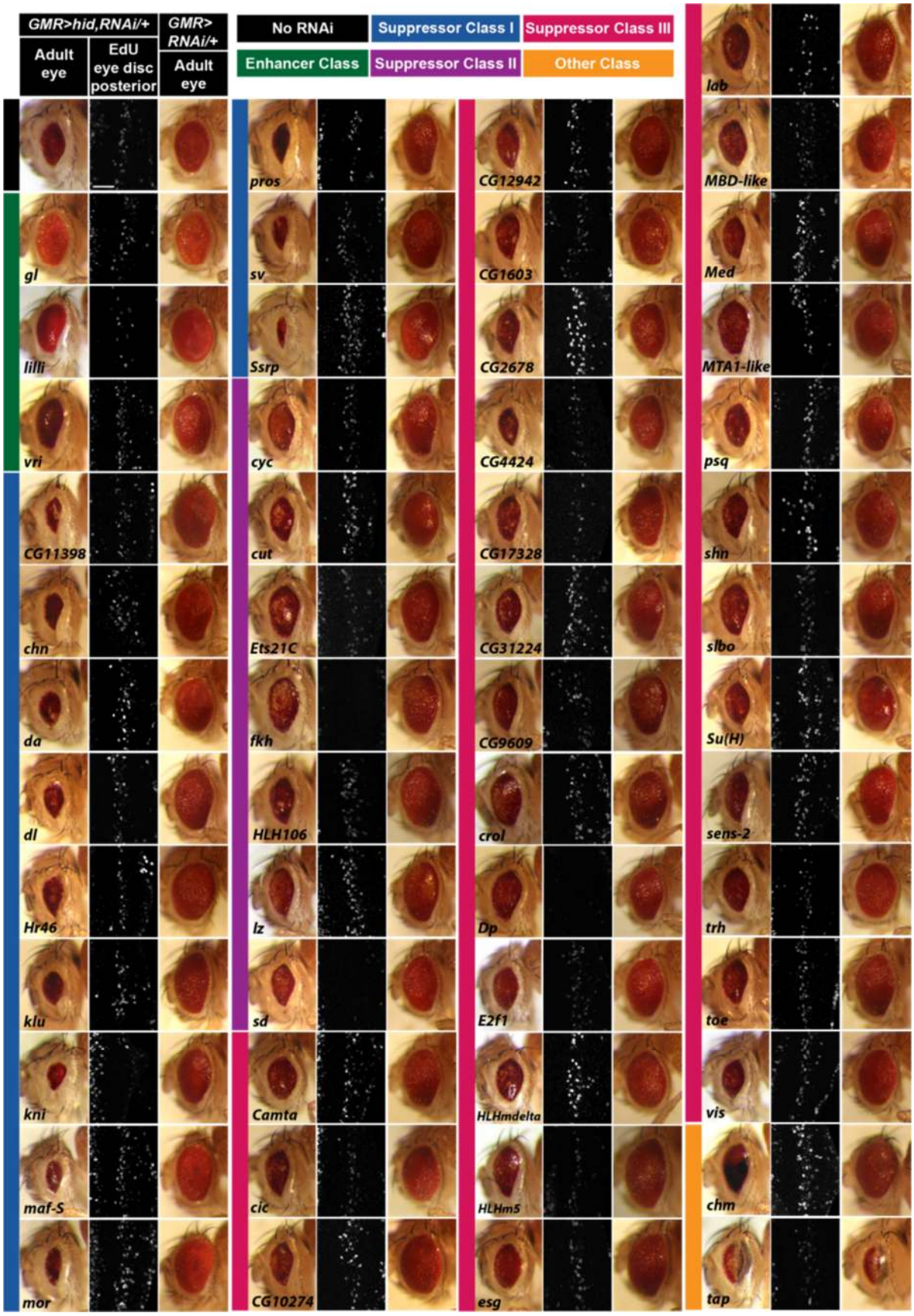
GMR>hid,RNAi/+
Adult eye
EdU eye disc posterior
GMR> RNAi/+
Adult eye
No RNAi
Suppressor Class I
Suppressor Class III
Enhancer Class
Suppressor Class II
Other Class
gl
lilli
vri
CG11398
chn
da
dl
Hr46
klu
kni
maf-S
mor
pros
sv
Ssrp
cyc
cut
Ets21C
fkh
HLH106
lz
sd
Camta
cic
CG10274
CG12942
CG1603
CG2678
CG4424
CG17328
CG31224
CG9609
crol
Dp
E2f1
HLHmdelta
HLHm5
esg
lab
MBD-like
Med
MTA1-like
psq
shn
slbo
Su(H)
sens-2
trh
toe
vis
chm
tap

Supp. Figure 4 (related to Fig. 2). 52 RNAi lines caused a change in the *GMR-hid* adult eye phenotype.

Each UAS-RNAi line was crossed to *GMR>hid, Gal4*. For each line, the adult eye phenotype is displayed in the left column, while the EdU staining of the posterior eye disc is displayed in the right column (centered on the compensatory wave; scale bar: 20 μM and magnification is the same throughout; anterior is oriented to the left). Each line was also crossed to *GMR-Gal4* alone (adult eye phenotype in third column). See Table S1 for full gene names and all RNAi lines tested. First row of images represents the "No RNAi" control. Phenotype classes (see text for explanation): Suppressors=green, Enhancer Class I=blue, Enhancer Class II=purple, Enhancer Class III=pink, Other=orange

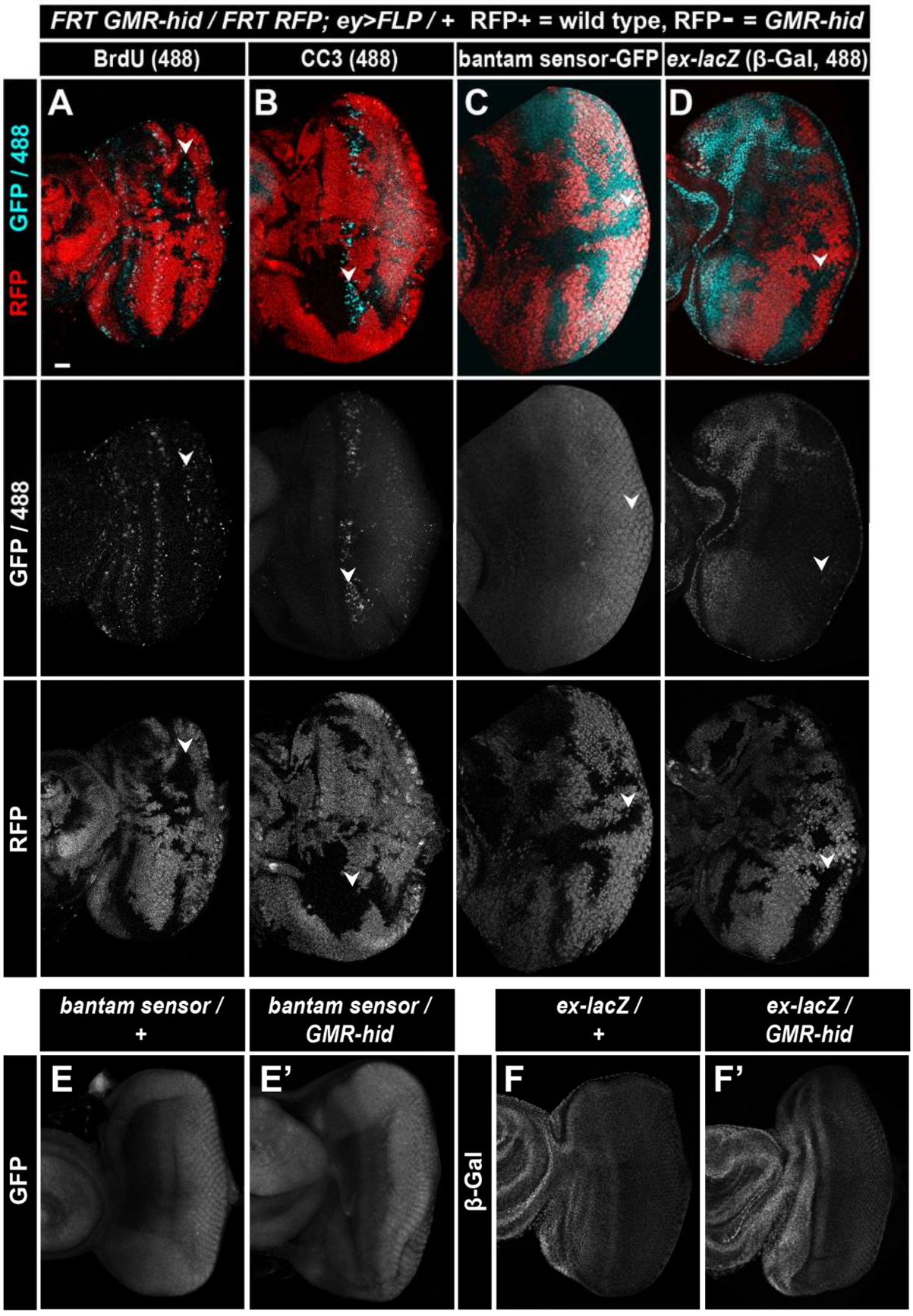
FRT GMR-hid / FRT RFP; ey>FLP / + RFP+ = wild type, RFP- = GMR-hid
BrdU (488)
CC3 (488)
bantam sensor-GFP
ex-lacZ (β-Gal, 488)
A
B
C
D
RFP GFP / 488
GFP / 488
RFP
bantam sensor / +
bantam sensor / GMR-hid
ex-lacZ / +
ex-lacZ / GMR-hid
E
E'
F
F'
GFP
β-Gal

Supp. Figure 5 (related to Fig. 4). A *bantam* sensor and *ex-lacZ* are not induced by *hid* expression in the eye disc.

A-D) *GMR-hid* clones (RFP negative, arrowheads) exhibit CP, marked by EdU (cyan, A), and apoptosis, marked by anti-CC3 staining (cyan, B). *bantam*, measured by the *bantam* sensor-GFP (cyan, C), and *ex-lacZ*, marked by β-Gal (cyan, D), are not induced in *GMR-hid* clones.

E) *bantam* sensor-GFP expression in control (E) and *GMR-hid* (E') eye discs.

F) *ex-lacZ* induction, marked by β-Gal, in control (F) and *GMR-hid* (F') eye discs.

Anterior is oriented to the left. Scale bars: 20 μM.

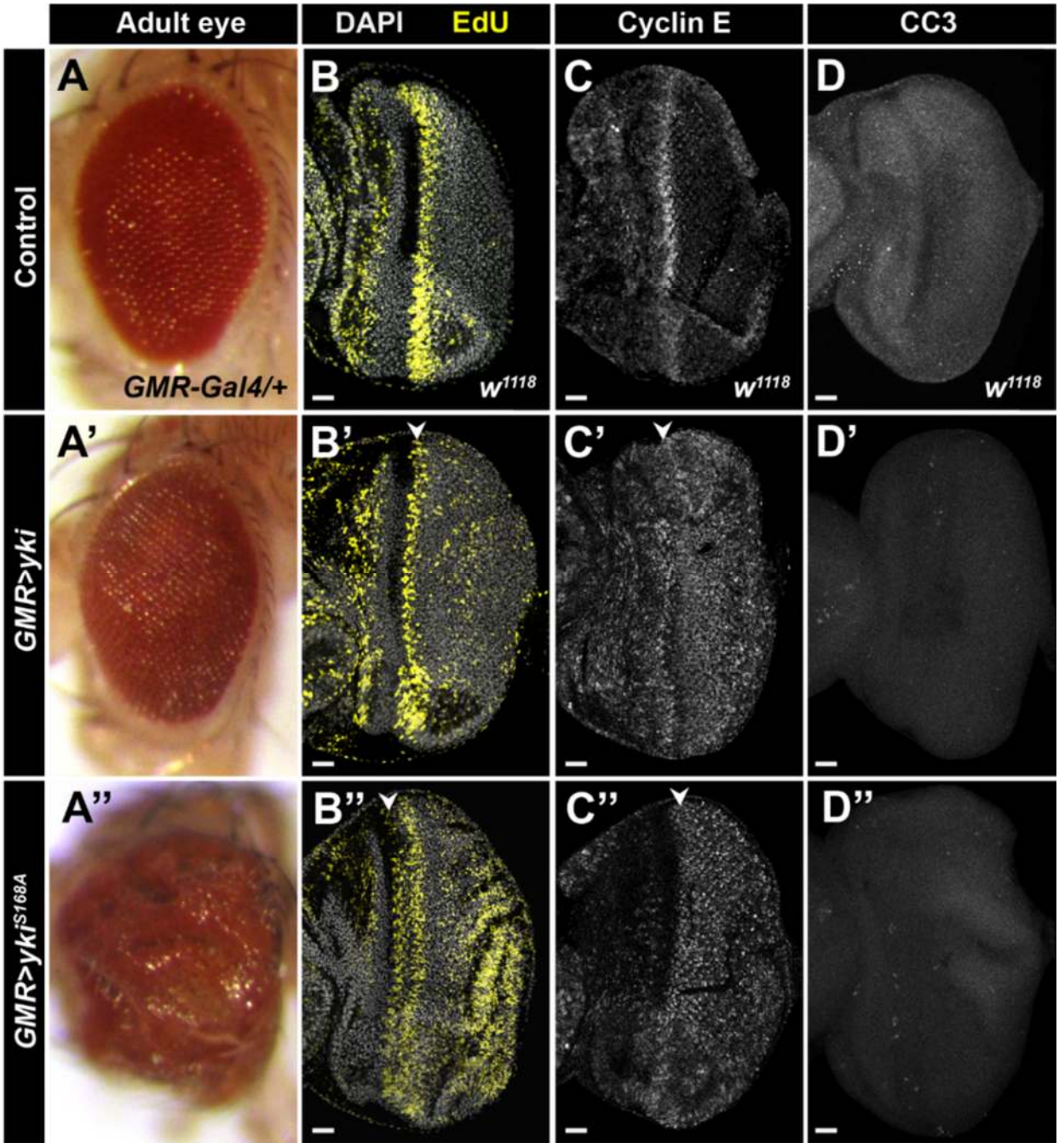

Supp. Figure 6 (related to Fig. 5). Expression of Yki or Yki^{S168A} induces larval and adult eye phenotypes.

A) Adult eyes with *GMR-Gal4* alone (A), with *UAS-Yki* (A'), or with *UAS-Yki^{S168A}* (A'').

B) DAPI staining of nuclei (grey) and EdU staining of S phase cells (yellow) in the indicated genotypes.

C) Staining with anti-Cyclin E antibodies in the indicated genotypes.

D) Staining of apoptotic cells with anti-CC3 antibodies in the indicated genotypes

Anterior is oriented to the left. Scale bars: 20 μM.

Supplementary Experimental Procedures

Fly stocks

RNAi lines used in the screen are listed in supplementary material Table S1. Additional fly stocks used are as follows, with full genotype and Bloomington Stock Center number or providing lab listed in parentheses: ***GMR-hid*** (*P{w[+mC]=GMR-hid}G1*, #5771), ***Tie RNAi*** (*y^1 v^1; P{TRiP.HMJ21428}attP40*, #54005), ***UAS-bsk^{DN}*** (made by K. Matsumoto, obtained from J. Poulton), ***UAS-puc*** (made by A. Martinez Arias, obtained from J. Poulton), ***puc-lacZ*** (*puc-lacZ^{E69}*, made by A. Martinez Arias, obtained from J. Poulton), ***luciferase (luc) RNAi*** (*y^1 v^1; P{TRiP.JF01355}attP2*, #31603), ***Cyclin E RNAi*** (*y^1 v^1; P{TRiP.JF02473}attP2*, #29314), ***UAS-p21*** (I. Hariharan), ***GMR-p21*** (*y^1 w^{1118}; P{GMR-p21.Ex}3/TM3, Sb^1 Ser^1*, #8414), ***sd RNAi-1*** (*y^1 v^1; P{TRiP.JF02514}attP2*, #29352), ***sd RNAi-2*** (*sd (N+C) RNAi*, J. Jiang), ***FRT sd*** (*FRT19A sd^{47m}*, D. Pan), ***FRT RFP*** (*P{Ubi-mRFP.nls}1, w^{1118}, P{neoFRT}19A*, #31416), **FRT GMR-hid; *ey>FLP*** (*P{GMR-hid}SS1, y^1 w* P{neoFRT}19A; P{GAL4-ey.H}SS5, P{UAS-FLP.D}JD2*, #5248), ***Tgi RNAi*** (*y^1 sc* v^1; P{TRiP.HMS00981}attP2*, #34394), ***yki RNAi-1*** (*y^1 v^1; P{TRiP.HMS00041}attP2*, #34067), ***yki RNAi-2*** (*y^1 v^1; P{TRiP.JF03119}attP2*, #31965), ***UAS-dMSTn*** (J. Jiang), ***bantam sensor*** (made by S. Cohen, obtained from T.T. Su), ***ex-lacZ*** (*w*; ex^{e1} P{neoFRT}40A/CyO*, #44249), ***Diap1-lacZ*** (*y^1 w*; P{lacW}Diap1^{j5C8}/TM3, Sb^1*, #12093), ***UAS-yki*** (*y^1 w^*; P{UAS-yki.GFP}4-12-1*, #28815), ***UAS-yki^{S168A}*** (*w*; P{UAS-yki.S168A.V5}attP2*, #28818), ***jub RNAi*** (*y^1 sc* v^1; P{TRiP.HMS00714}attP2*, #32923), ***jub-GFP*** (*w^*; P{jub$^{+t.T:Avic\GFP}$}18A/TM2*, #56806), ***UAS-RokCAT*** (*y^1 w*; P{UAS-Rok.CAT}3.1*, #6669), ***UAS-Cdc42^{DN}*** (*w^*; P{UAS-Cdc42.N17}3*, #6288).

Genotypes for clones are as follows:

sd clones: *FRT19A sd^{47m}/FRT19A Ubi-mRFP.NLS; GMR-hid/+; ey-Gal4, UAS-FLP/+*

GMR-hid clones: *FRT19A GMR-hid/FRT19A Ubi-mRFP.NLS; ey-Gal4, UAS-FLP/+*

GMR-hid clones with *bantam* sensor: *FRT19A GMR-hid/FRT19A Ubi-mRFP.NLS; bantam sensor GFP/+; ey-Gal4, UAS-FLP/+*

GMR-hid clones with *ex-lacZ*: *FRT19A GMR-hid/FRT19A Ubi-mRFP.NLS; ex-lacZ/+; ey-Gal4, UAS-FLP/+*

jub-GFP clones: FRT19A GMR-hid/FRT19A Ubi-mRFP.NLS; jub-GFP/ey-Gal4, UAS-FLP

longGMR-hid transgene construction

To make *longGMR-hid* transgenic flies, the *longGMR* (*LGMR*) enhancer and *hid* ORF were cloned into pMINTGATE, a kind gift from J. Pearson. *LGMR-Gal4* transgene was obtained by PCR amplification from *LGMR-Gal4* flies (Bloomington #8121) with primers white 2161 (forward, GTGTCGCTCGTTGCAGAATA) and Gal4R (reverse, GCCTTGATTCCACTTCTGTCA). The *longGMR* enhancer was then PCR'ed from this fragment with primers LGMRpE F (forward, CACCCAAGCTTTCGCGAGCTCG) and LGMRpE R (reverse, TTTCGCCGGATCTCGACAATAG) and cloned into pENTR/D-TOPO (Invitrogen); pENTR LGMR was then recombined into pMINTGATE using the Gateway LR cloning system (Invitrogen), resulting in pMG LGMR. The *hid* ORF (sequence from BDGP clone AT13267) was synthesized by GenScript with AgeI and SpeI sites for cloning into pMG LGMR, which replaced the *GFP*, but retained the plasmid's SV40 3'UTR. The resulting construct (pMG LGMR hid) was injected by BestGene Inc into the attP40 site to make transgenic flies.

Image quantification

ImageJ (NIH) was used for all quantification. For all statistical measurements, p-values were calculated using the T-test function in Microsoft Excel with two-tailed distribution and two-sample unequal variance.

Measurement of SMW to CP distance

Z-projections were made in ImageJ of EdU staining in control (*GMR>hid, luc RNAi*) or experimental (*GMR>hid, yki*) eye discs. From these images, the physical distance from the anterior edge of the SMW to the anterior edge of the CP wave was measured. To

mitigate confounding effects from preparation artifacts at the dorsal and ventral edges of the disc (e.g. curling over), the distance between the SMW and CP was measured at the approximate midpoint (determined qualitatively) along the D-V axis. In all cases, the farthest distance was measured. Since the CP wave is not entirely synchronous, single EdU^+ cells considerably anterior to other cells in the wave (>10 μM away) were considered anomalies and were not considered in our determination of the anterior CP edge.

Cleaved-Caspase 3 staining

For cleaved Caspase-3 staining quantification, projections of images with anti-CC3 antibody staining were used to calculate total disc area in ImageJ (Huang thresholding to capture entire disc, followed by measurement of total area of particles >100 pixels, which in all cases was one particle, ie the whole disc) and area of CC3 posterior to the furrow (RenyiEntropy thresholding to capture CC3 staining, followed by measurement of total area of particles >3 pixels, which were all cells with CC3 staining). Thresholding was set manually to account for differences in background and signal between samples. Area was used as a measurement rather than total number of $CC3^+$ cells as fragmented cells with pyknotic nuclei could not be unambiguously counted as one or multiple cells. The total area of the disc was used to normalize the area of CC3 staining so that the measurement of CC3 staining is displayed as a percent of total disc area.

Diap-lacZ / β-Gal staining

β-Gal staining from discs with *Diap-lacZ* expression was quantified by calculating the ratio of average intensity of staining posterior and anterior to the furrow. For posterior measurements, a selection containing at least 50 undifferentiated cells (identified by their location apical to the glial cells) in a single slice was made posterior to the furrow. This selection specifically did not include any glial, peripodial, margin, or pre-furrow nuclei, which could confound our measurements. DAPI staining was used to create a ROI containing nuclei. β-Gal fluorescence intensity was then measured in this nuclear ROI. A similar measurement was made with cells anterior to the furrow to normalize differences

in staining between samples. The ratios of average nuclear β-Gal intensity in posterior versus anterior disc cells were used to compare genotypes.

Cyclin E staining

Because staining with anti-Cyclin E antibodies is variable throughout the posterior of eye discs, presumably due to differences in Cyclin E protein accumulation, in each disc we measured the average Cyclin E staining intensity for undifferentiated cells, where differences between genotypes appeared greatest. Since fluorescence from glial, peripodial, or photoreceptor cells could confound our measurements, we gated for undifferentiated cells by applying a mask of Yan staining to Z-stacks of Cyclin E staining. A maximum projection was generated from each gated Cyclin E Z-stack. The resulting image of Cyclin E staining in undifferentiated cells was thresholded using cells with high Cyclin E levels in the SMW as a reference point for Cyclin E positive cells. Since nuclei could not be separated in Z-projected images, area was used as a proxy for cell number. The area of Cyclin E positive cells posterior to the SMW was normalized to the area of Cyclin E positive cells within the SMW. The measurements displayed in Figure 4 and used for quantification are a ratio of post-SMW versus SMW Cyclin E staining area. We considered that the SMW Cyclin E area itself might be different between genotypes, especially considering that Hid expression disrupts the SMW. Therefore, we also measured the area of Cyclin E positive cells posterior to the SMW as a percentage of the total posterior area, based on projections of Yan staining. Statistical comparisons of percent of total posterior disc area with Cyclin E staining for each genotype gave similar significant P-values as our post-SMW versus SMW ratios. We chose to display the post-SMW versus SMW ratios in our results as we feel these measurements better account for differences in staining efficiency than post-SMW area alone.

Table S1.

Click here to Download Table S1